The role of the cystic fibrosis transmembrane conductance regulator in host protection against *Citrobacter rodentium* intestinal infection

Travis Ackroyd

Department of Microbiology and Immunology

McGill University, Montreal

August 2016

A thesis submitted to McGill University in partial fulfillment of the requirements of the degree of Master of Science

Abstract

Cystic fibrosis (CF) is a fatal disease caused by mutations in the cystic fibrosis transmembrane conductance regulator (*CFTR*) gene. Located in the membrane of various epithelial tissues and immune cells, CFTR plays a critical role in ion and fluid homeostasis. Although often associated with a respiratory phenotype, CF affects the gastrointestinal tract. Mouse models of CF display little lung pathology, but do possess an intestinal phenotype, characterized by obstruction, inflammation, and bacterial overgrowth.

We have shown that ΔF508 CF mice (*Cftr*^{tm1Eur}) are highly susceptible to intestinal infection with *Citrobacter rodentium*, with atypical localization and greater colonization of bacteria than WT mice. Notably, there are significantly more neutrophils in the small intestine of CF mice both at steady state and following infection. Despite this increase, we have shown that CF neutrophils are defective in reactive oxygen species (ROS) production and have decreased apoptosis compared to WT. CF mice also have altered Wnt signaling at steady state, with increased active β-catenin in the intestinal stromal cell compartment.

To determine the relative contributions of the *Cftr*-deficient myeloid and epithelial cell compartments to infection susceptibility, we generated mice with myeloid-specific *Cftr* inactivation. Myeloid-*Cftr*$^{-/-}$ mice were resistant to infection with no defects in myeloid cell ROS production or apoptosis. We are now generating mice with *Cftr* inactivation in the intestinal epithelium, to test the hypothesis that functional CFTR mediates its protection in an intestinal epithelial cell dependent manner.

C. rodentium infection provides a model to study intestinal disease observed in CF patients. Furthermore, the lack of a robust mouse model of CF pulmonary disease renders our research important for the study of the role of CFTR at mucosal surfaces.

Résumé

La fibrose kystique (FK) est une maladie mortelle causée par des mutations dans le gène *cystic fibrosis transmembrane conductance regulator* (*CFTR*). La protéine CFTR, exprimée dans plusieurs cellules épithéliales et immunitaires, joue un rôle critique dans le maintien de l'homéostasie ionique et des liquides aux membranes cellulaires auxquelles se localise la protéine. Alors que la maladie touche surtout l'appareil respiratoire, les organes de la voie digestive sont aussi affectés. En revanche, les souris modèles de la maladie de FK ne démontrent que très peu de pathologies respiratoires, tout en possédant un important phénotype intestinal caractérisé par l'obstruction, l'inflammation et l'excroissance bactérienne.

Nous avons démontré que la souris de FK, porteuse de la mutation ΔF508 (*Cftr*^{tm1Eur}), est très susceptible à l'infection intestinale par la bactérie *Citrobacter rodentium*, et est caractérisée par une plus grande colonisation bactérienne à des endroits atypiques comparativement aux souris sauvages. Notamment, nous avons observé autant chez les souris de FK stables et infectées une augmentation significative du nombre de granulocytes neutrophiles dans l'intestin grêle. Malgré leur prolifération, les granulocytes neutrophiles de FK sont marqués par une diminution en apoptose, et ne peuvent déclencher la production de dérivés réactifs de l'oxygène (DRO), comparativement aux souris sauvages. De plus, le stroma de l'intestin affiche une hausse en β-caténine active, ce qui témoigne d'une altération de la cascade de signalisation Wnt à l'état stable.

Afin d'évaluer la contribution relative de chaque compartiment cellulaire à la susceptibilité à l'infection, c'est-à-dire les compartiments myéloïdes et épithéliaux dépourvus du gène *Cftr*, nous avons créé des souris transgéniques porteuses du gène *Cftr* invalidé uniquement dans le compartiment myéloïde. Ces souris myéloïdes-*Cftr*$^{-/-}$ ont résisté l'infection et leurs cellules myéloïdes n'ont présenté aucun défaut en apoptose et en production de DRO. Dans le but

d’adresser notre hypothèse qu’une protéine CFTR fonctionnelle pourrait conférer un effet protecteur au niveau de l’épithélium intestinal, nous travaillons actuellement à produire des souris porteuses du gène *Cftr* invalidé seulement dans les cellules épithéliales de l’intestin.

L’infection au *C. rodentium* est un modèle bien adapté à l’étude de la maladie intestinale observée chez les patients de FK. Notre travail sur la fonction de CFTR aux surfaces muqueuses est essentiel en l’absence d’un modèle murin fiable qui permettrait l’étude de l’aspect pulmonaire de la maladie de FK.

Table of Contents

List of Abbreviations

ABC	ATP binding cassette
A/E	attaching and effacing
AMP	antimicrobial peptide
ATP	adenosine triphosphate
cAMP	cyclic adenosine monophosphate
BSA	bovine serum albumin
BMDM	bone marrow derived macrophage
CF	cystic fibrosis
CFTR	cystic fibrosis transmembrane conductance regulator
CRC	colorectal cancer
DAPI	4', 6'-diamidino-2-phenylindole
DC	dendritic cell
DHR	dihydrorhodamine 123
DIOS	distal intestinal obstructive syndrome
DPI	days post-infection
EHEC	enterohemorrhagic *Escherichia coli*
ENaC	epithelial sodium channel
EPEC	enteropathogenic *Escherichia coli*
EPI	exocrine pancreatic insufficiency
FABP	fatty acid-binding gene promoter
FCS	fetal calf serum
GI	gastrointestinal
GM-CSF	granulocyte-macrophage colony-stimulating factor
GSH	glutathione
H&E	hematoxylin and eosin
HBSS	Hanks balanced salt solution
HOCl	hypochlorous acid
i.v.	intravenous
IEC	intestinal epithelial cell
IgE	immunoglobulin E
IL	interleukin
ILC	innate lymphoid cell
IVIS	*in vivo* imaging system
LB	Luria-Bertani
LEE	locus of enterocyte effacement
LPS	lipopolysaccharide
Lrg	leucine-rich α2 glycoprotein
M cell	microfold cell

MCSF	macrophage colony stimulating factor
MI	meconium ileus
MMC	migrating motor complex
NBD	nucleotide binding domain
NFAT	nuclear factor of activated T-cells
NLR	NOD-like receptor
PAMP	pathogen-associated molecular pattern
PCNA	proliferating cell nuclear antigen
PKA	protein kinase A
PMA	phorbol 12-myristate 13-acetate
PRR	pattern-recognition receptor
REGIIIβ	regenerating islet-derived protein 3 beta
REGIIIγ	regenerating islet-derived protein 3 gamma
RLR	RIG-I-like receptor
ROS	reactive oxygen species
R region	regulatory region
RSPO2	R-spondin 2
SCN-	thiocyanate
SIBO	small intestinal bacterial overgrowth
T3SS	type III secretion system
TGFβ	transforming growth factor β
Th cell	helper T-cell
TLR	Toll-like receptor
TMD	transmembrane domain
TNF	tumor necrosis factor
WT	wild type
ZymTR	Zymosan-Texas-Red

List of Figures and Tables

Acknowledgments

First and foremost, I would like to thank my supervisor, Dr. Samantha Gruenheid, for all of her help throughout the completion of my thesis. Without her unwavering support, guidance, and wealth of experience, I wouldn't have grown into the scientist that I am today. I am grateful to consider her as both a mentor and a friend. All lab members were critical components of my project. In particular, I would like to thank Dr. Mitra Yousefi for her assistance with the immunology components of my thesis. Her hard work and innovation did not go unnoticed. Also, thank you to Lei Zhu for her expert technical assistance with mouse colony maintenance and infections. Lastly, thank you to Eugene Kang for teaching me techniques and providing an extra hand when needed.

I would like to acknowledge my committee members, Dr. John Hanrahan and Dr. Jörg Fritz, who provided me with the advice and criticism necessary to shape my project. I am thankful to two members of their labs, Jie Liao and Barbara Mindt respectively, for their contributions to my project.

The Complex Traits Group at McGill became a home for me and I was fortunate to spend my time with brilliant and caring people. I would like to highlight my friendship with Jessica Petrov and Rupinder Boora - thank you for making the best out of any situation and for being like sisters to me. Thank you to Mathieu Mancini for his scientific input, translation of my abstract, and the endless witty banter. Finally, despite our short time together at the CTG, I would like to thank Caitlin Schneider for her help with injections and for being an extension of my personality.

Lastly, I cannot say enough about the love and support my parents have shown me in pursuit of my goals.

Chapter 1: Literature Review

1.1 Cystic fibrosis

1.1.1 Cystic fibrosis as a human disease

Cystic fibrosis (CF) is a fatal autosomal recessive disorder for which there is currently no cure [1]. CF is the most common genetic disorder among Caucasian populations, affecting approximately 1 in every 2500 live births [1]. Although fatal, the average life expectancy of CF patients has risen dramatically over past decades to 37 years of age [2]. CF is a systemic disease consistently characterized by progressive lung disease and chronic digestive problems [3]. Though the severity of symptoms differs between patients based on genetic and environmental factors, the majority of CF pathology results from mucus accumulation along epithelial surfaces, leading to obstruction, infection, and inflammation [4, 5].

The fundamental cause of CF is mutation in the cystic fibrosis transmembrane conductance regulator gene (*CFTR*), encoding a cyclic adenosine monophosphate (cAMP) regulated ion channel [6]. Found in the apical membrane of various epithelia, as well as immune cells, the main role of CFTR is in anion secretion, particularly chloride and bicarbonate. Defects in CFTR function result in lack of ion and water homeostasis at epithelial surfaces [7].

1.1.2 The cystic fibrosis transmembrane conductance regulator

The gene encoding for CFTR is located on chromosome 7 and is highly conserved among mammalian species [8]. The CFTR protein is a member of the adenosine triphosphate (ATP) binding cassette (ABC) transporter family, characterized by the use of ATP hydrolysis to pump

its substrates across cellular membranes [9]. CFTR is the only known ABC protein that functions as an ion channel [10].

Although there is currently no high resolution X-ray crystal structure for full length CFTR, the general arrangement of the protein within the apical membrane of epithelial cells has been described [11]. Similar to the architecture of other ABC transporters, CFTR has two transmembrane domains (TMDs) and two nucleotide-binding domains (NBDs) for ATP-binding [9]. Each TMD consists of six membrane-spanning helices through which ions are allowed to pass [10]. Unique to CFTR is the presence of a highly charged regulatory region (R region). The R region contains nine consensus sequences for protein kinase A (PKA) phosphorylation and is critical in the opening of CFTR [3]. Together, these domains fuse together and form a single polypeptide chain, resulting in a 1480-residue long membrane protein [9].

Activation of CFTR occurs in a sequential order and follows the ATP Switch model [13]. A presumptive model of CFTR structure and function is outlined in Figure 1 [14]. In general, binding of the substrate (chloride and bicarbonate) to the TMDs facilitates ATP-binding at the NBDs [13]. ATP-dependent dimerization of the NBDs releases the substrate from the TMDs and ATP hydrolysis destabilizes the NBD closed dimer [13]. Following release of inorganic phosphate, PKA phosphorylates the R region of CFTR in a cAMP-dependent manner, leading to its activation [15]. Once activated, chloride and bicarbonate ions can move freely through the channel formed by the TMDs in the apical membrane [14]. Under normal conditions, this movement of anions out of the cell is accompanied by paracellular transport of water and sodium across the epithelium and into the lumen [16]. Furthermore, the inhibition of apical sodium

channels, as well as the co-activation of basolateral potassium channels, is concurrent to CFTR activation and helps to maintain an electrochemical gradient for chloride and bicarbonate out of the cell [16].

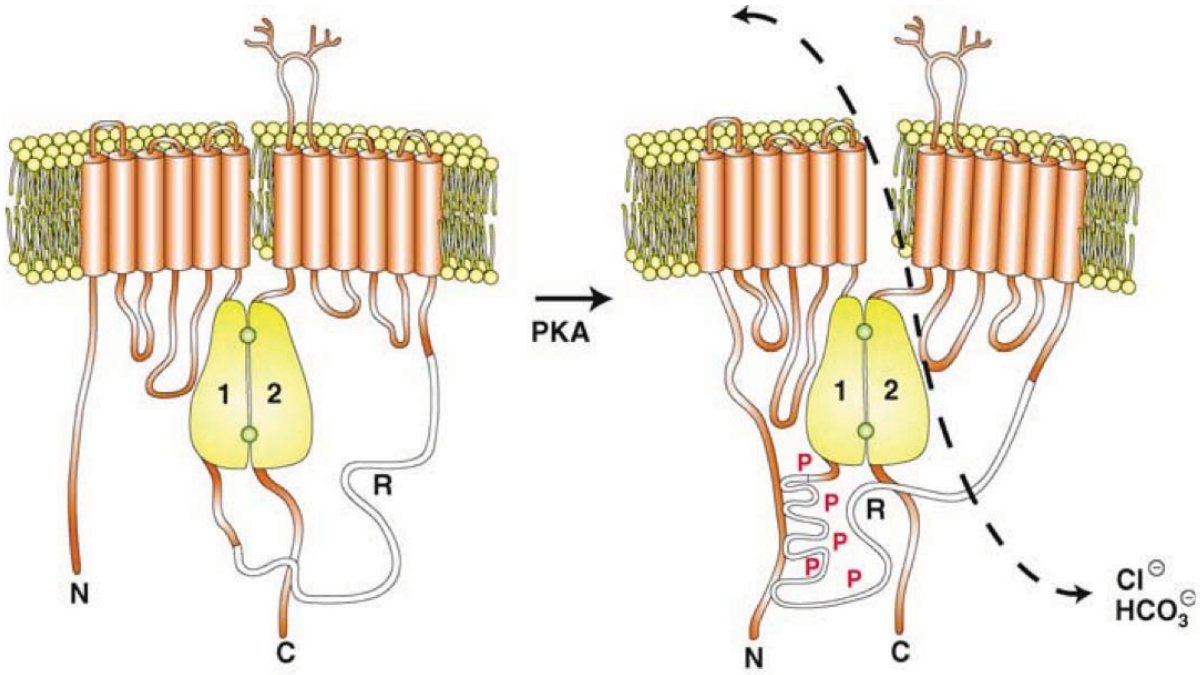

Figure 1. PKA-dependent phosphorylation of the R region leads to CFTR opening.
Cartoon summary of PKA-dependent phosphorylation of the R domain of CFTR. Once phosphorylated, the R domain of CFTR is speculated to interact with the amino-terminus, resulting in channel opening. Chloride and bicarbonate ions are then allowed to pass through the TMDs of CFTR in the epithelium. [14]

1.1.3 CFTR mutations

Currently, over 1900 mutations of *CFTR* have been described and comprise five different classes based on the molecular mechanism of CFTR disruption [17, 18]. Class I mutations result in a premature stop codon and defective protein synthesis. Class II mutations are defective in protein folding, and are targeted for degradation prior to translocation to the plasma membrane [18]. Class III and IV mutations reach the plasma membrane, but are defective in channel opening and channel conductance, respectively [18]. Lastly, class V mutations are fully functional proteins

present at lower abundance [18]. Generally, classes I-III cause more severe phenotypes, whereas classes IV and V are milder [18].

The most common mutation in human CF disease is a Class II mutation within exon 10, encoding for the first NBD of CFTR [19]. More specifically, it is a deletion of a phenylalanine residue at position 508 (ΔF508), leading to protein misfolding and targeted degradation via the proteasome [20]. This mutation destabilizes the structure and folding of CFTR, and results in less than 1% of translated protein at the plasma membrane [21]. Greater than 70% of CF patients suffer from the ΔF508 mutation, making it the most studied and clinically relevant CF genotype [22].

1.2 The cystic fibrosis immune system

Humans with CF and murine models of the disease have an exaggerated immune response in both the absence and presence of pathogenic stimuli [23]. Characterization of the CF immune system has largely focused on airway inflammation during bacterial infection, and will be reviewed here.

1.2.1 Innate immunity in cystic fibrosis

The innate immune system is a critical component in the initial host response to infection [24]. However, despite an exaggerated innate response in the CF lung, characterized by considerable neutrophil influx, airway inflammation is often ineffective at pathogen control [23]. An overview of the immune response to bacterial infection in the airway epithelial cells of CF patients is outlined in Figure 2 [23].

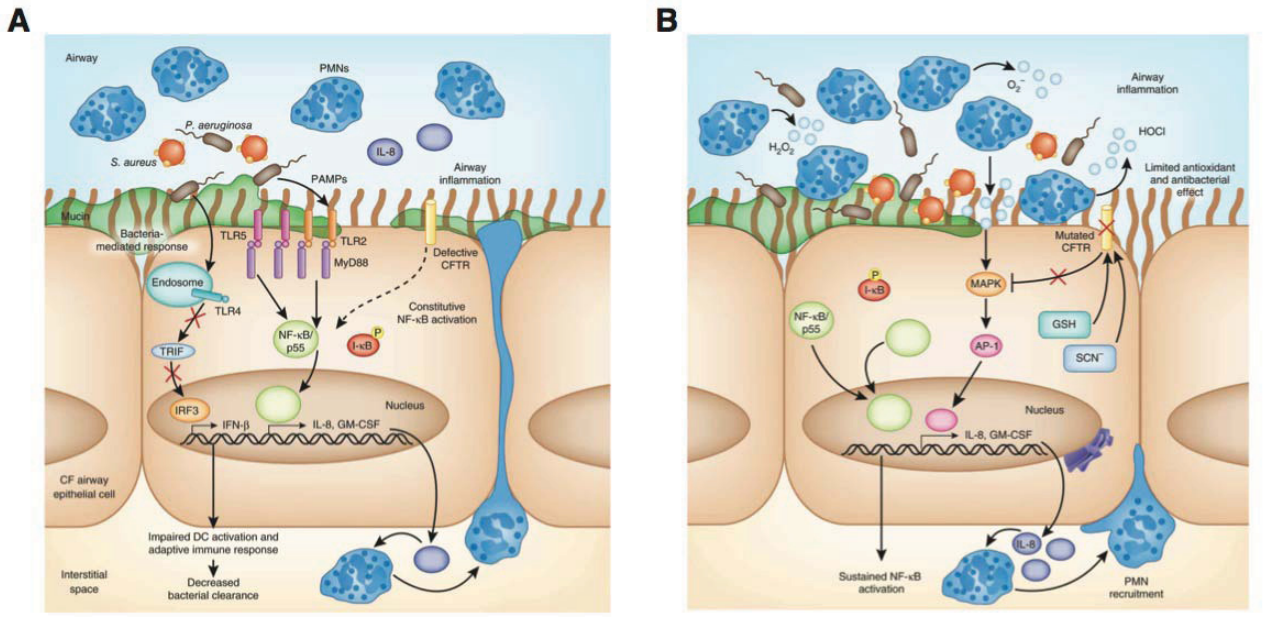

Figure 2. CF immune response to bacterial infection in airway epithelial cells.
(A) Altered TLR expression in the CF airway epithelium leads to constitutively activated NF-κB and increased IL-8 and GM-CSF production. This pathway can be potentiated by bacterial colonization, ultimately resulting in increased neutrophil recruitment. Also, TLR4 expression is restricted to the endosome and activation of Trif from the endosome is impaired. As such, type I IFN gene products required for DC activation are impaired. **(B)** The persistent neutrophilic response in the CF lung results in increased oxidative stress, activating MAPK signaling and amplifies IL-8 and GM-CSF production. Channeling of the antioxidants GSH and SCN^- is defective in the CF airway, making the epithelium unable to counteract oxidative stress. [23]

Defective CFTR in the airway epithelium results in constitutive NF-κB activation and release of MAPK inhibition [25, 26]. Together, these signaling pathways are critical in the transcription of the proinflammatory molecules Interleukin (IL) - 8 and granulocyte-macrophage colony-stimulating factor (GM-CSF) [23]. During microbial infection, these signaling pathways are augmented by pathogen-associated molecular pattern (PAMP) recognition via Toll-like receptors 2 (TLR2) and 5 (TLR5) [27]. TLR2 and TLR5 begin a signaling cascade through the MyD88 adaptor protein to further induce NF-κB activation [27]. Collectively, the resulting increase in IL-8 and GM-CSF stimulates neutrophil recruitment across the epithelium [28, 29].

ROS production by recruited neutrophils is typically an effective method of pathogen control [30]. However, mutated CFTR is unable to transport glutathione (GSH) and thiocyanate (SCN^-) across the epithelium and into the epithelial-lining fluid [31, 32]. Considering both GSH and SCN^- are antioxidants that help to control oxidative damage, the CF lung has a diminished capacity to counter neutrophil-associated oxidative stress [23, 33]. As a result, there is increased tissue destruction and pathology in the CF lung, with diminished anti-microbial killing [23]. Furthermore, increased oxidative stress causes a positive feedback loop that increases IL-8 transcription and potentiates the neutrophil response [34].

In addition to increased oxidative damage of the lung architecture, other defects in CF neutrophil function have been well documented. CF neutrophils have been shown to have increased proteolytic degradation of elastin, further contributing to the disruption of lung function [35]. These neutrophils also have decreased motility, phagocytosis, and apoptosis, compared to healthy controls [36, 37, 38].

Although epithelial disruption of CFTR function accounts for the majority of CF morbidity, the intrinsic effect of mutant CFTR on immune cells has yet to be determined [39]. Previous studies on CF inflammation have worked largely with primary epithelial cells and may be lacking critical interactions with immune cells [39]. However, whether CFTR is present within immune cells, and in particular neutrophils, remains controversial and poorly defined [40].

One group demonstrated that mutated CFTR in neutrophils affects the expression of approximately 89 different genes [41]. They hypothesized that defective chloride secretion in CF

neutrophils could result in increased intracellular calcium, which has been shown to alter inflammatory gene expression pathways [41]. Furthermore, myeloid-specific *Cftr*$^{-/-}$ mice have been shown to have decreased hypochlorous acid (HOCl) and microbial killing compared to controls [42]. These mice also had intermediate susceptibility to *Pseudomonas aeruginosa* lung infection when compared with wild type (WT) and *Cftr*$^{-/-}$ mice, highlighting a protective role of CFTR in the myeloid cell compartment [42]. Typically, neutrophils in the full *Cftr*$^{-/-}$ airway also have defective chlorination of phagocytosed bacteria with HOCl, further suggesting that loss of CFTR within neutrophils contributes to a defective immune response [43].

1.2.2 Adaptive immunity in cystic fibrosis

Despite a predominately innate immune response, CF patients also have alterations in adaptive immunity with a bias towards a helper T-cell (Th) 2 and 17 phenotype [44, 45, 46].

Th2 cells are generally regarded as mediators of an allergic response and are potent producers of IL-4, IL-5, and IL-13 [47, 48]. Although the mechanism of the Th2 bias in CF is not fully understood, aberrant calcium responses could conceivably lead to increased nuclear localization of nuclear factor of activated T-cells (NFAT), a transcriptional regulator of Th2 cytokines [49]. Murine studies have also supported the Th2 bias; with T-cell-specific *Cftr*$^{-/-}$ mice producing increased basal immunoglobulin E (IgE) [49]. Such a strong Th2-skewed immune response in CF patients could potentially counteract a Th1-mediated anti-microbial response.

Th17 cells are present in mucosal tissues and play a critical role in mucosal maintenance and pathogen clearance, especially extracellular bacteria [50]. Increased levels of IL-17 and IL-23,

regulators of Th17 development, have been observed in the sputum of CF patients compared to healthy controls [51]. Furthermore, IL-17^{+} Th17 cells have been shown to be the major source of exaggerated IL-17 production in the CF airway [52]. Also, naïve T-cells from the peripheral blood of CF patients are predisposed to a Th17 phenotype, as opposed to Th1 or regulatory T cells [53]. In some cases, a potent and uncontrolled Th17 response could be detrimental rather than protective, and could have negative implications on patient health [54]. Although an increase in Th17 cells has been demonstrated, the molecular pathway through which CFTR mediates Th17 differentiation remains to be elucidated.

1.3 Intestinal epithelial cells; structure and barrier function

Intestinal epithelial cells (IECs) protect mammalian hosts from the external environment and play a critical role in segregation between host and microbial communities [55]. As the body's largest mucosal surface, the intestinal epithelium maintains both a physical and biochemical barrier that protects the host from infiltration of both normal microflora and potential pathogenic species [56]. Furthermore, the coordinated effort of IECs can influence the immune system and provide additional host protection [57].

In general, the small intestine is organized into repeating invaginations (crypts) and projections (villi) of the intestinal epithelium. [56] Although crypts are present in the large intestine (colon), there are no villi present in that tissue [56]. The intestinal epithelium is comprised of a diverse set of cell types that function together to maintain barrier function and integrity [56]. These cells arise from pluripotent intestinal epithelial stem cells that reside in the base of intestinal crypts [58, 59]. Predominant cell types within the intestinal epithelium are highlighted in Figure 3 [56].

The majority of cells that border the intestine are absorptive enterocytes, primarily adapted for efficient digestion and other metabolic processes [55]. However, several other specialized IECs exist and have varying secretory function.

Enteroendocrine cells influence digestive processes through secretion of numerous hormones and hormone regulators [56]. Goblet cells secrete highly glycosylated mucins into the intestinal lumen that function as the first line of defense against infiltrating microbes [60]. In particular, MUC2 is the most abundant of the intestinal mucins and is essential for proper organization of intestinal mucus [61]. Antimicrobial peptides (AMPs) are secreted into the lumen by Paneth cells, which are located in the crypts of the small intestine and are unique to this region [62]. Although enterocytes are capable of secreting some AMPs, Paneth cells are the dominant IEC type with antimicrobial function [56]. Paneth cells produce defensins, cathelicidins and lysozymes, which each disrupt highly conserved features of bacterial biology [63]. Together, secretory IECs comprise a dynamic barrier that limits the quantity of bacteria that can reach the epithelial surface or penetrate deeper into the underlying mucosa [56].

IECs express pattern-recognition receptors (PRRs) that enable them to sense microbial stimuli and the surrounding environment to facilitate the coordination of an appropriate immune response. Distinct pathways capable of recognizing various microbial ligands exist and are comprised primarily of members of the TLR, NOD-like receptor (NLR), and RIG-I-like receptor (RLR) families [64, 65, 66, 67, 68]. These families often initiate signaling cascades that can lead to the activation of proinflammatory molecules [56]. Also, specialized IECs called microfold

cells (M cells) can sample luminal antigens and present them to the underlying immune system [69].

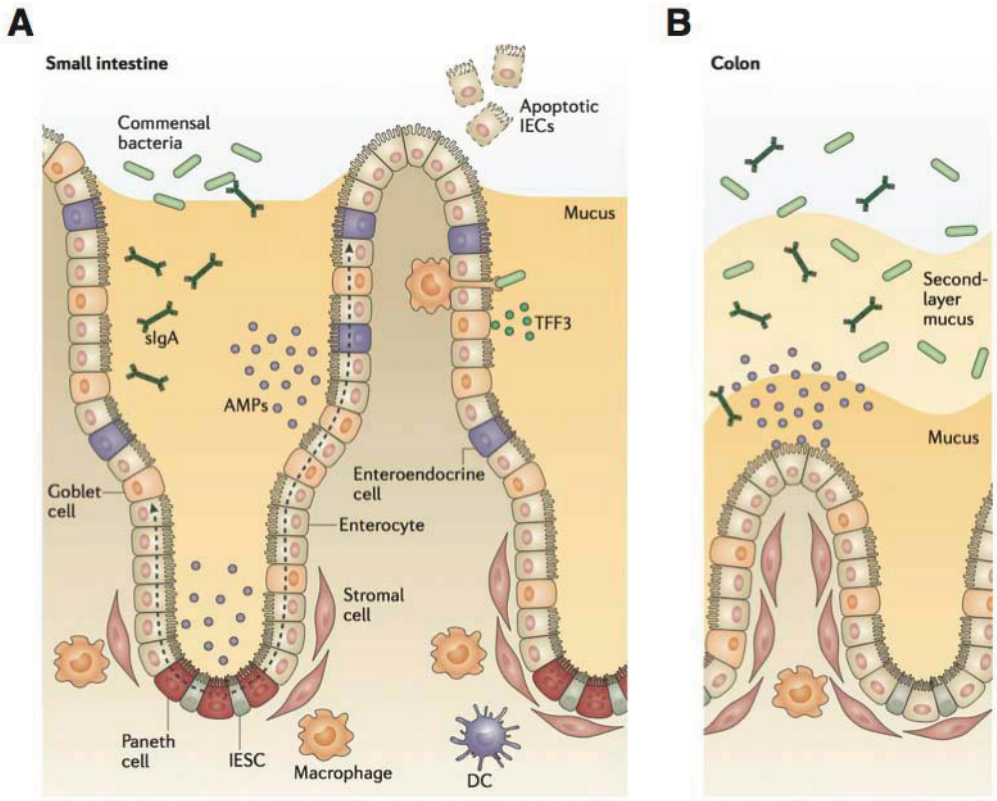

Figure 3. Structure of the intestinal epithelium.
Intestinal epithelial cells (IECs) form a barrier that separates the host intestinal lamina propria (hematopoietic and stromal cells) from microbial communities. Differentiated IECs arise from pluripotent intestinal epithelial cells in intestinal crypts. **(A)** The small intestine epithelium is comprised of enterocytes and specialized cell types that form crypts and villi. Some of the specialized cell types include Enteroendocrine cells, Goblet cells, and Paneth cells. **(B)** The large intestine (colon) is comprised of enterocytes and Goblet cells that form crypt architecture.

Collectively, IECs act as central mediators of microbial and immune homeostasis in the intestine and comprise a major facet to host protection.

1.4 Intestinal complications in cystic fibrosis

Although commonly associated with a respiratory phenotype and chronic lung infection, CF is a multi-organ disease with manifestations in multiple organ systems, including the gastrointestinal (GI) tract [70]. The gene expression of CFTR within the lower GI tract is outlined in Figure 4 [71]. CFTR expression is low within the stomach, but raises to higher levels in the intestine [72]. There is a gradient of CFTR expression in the intestine, with mRNA levels highest in the duodenum and decreasing distally to the large intestine [71]. Although lower, CFTR expression in the large intestine is still considered moderate [73]. This pattern of expression has been proposed to reflect the need for acid neutralization from the stomach with bicarbonate [71]. Furthermore, there is also a gradient of CFTR expression along the crypt-villus axis, with greatest expression near the base of the crypts in both the small and large intestine [71]. Importantly, the distribution of CFTR message is consistent with protein distribution in the GI tract [74].

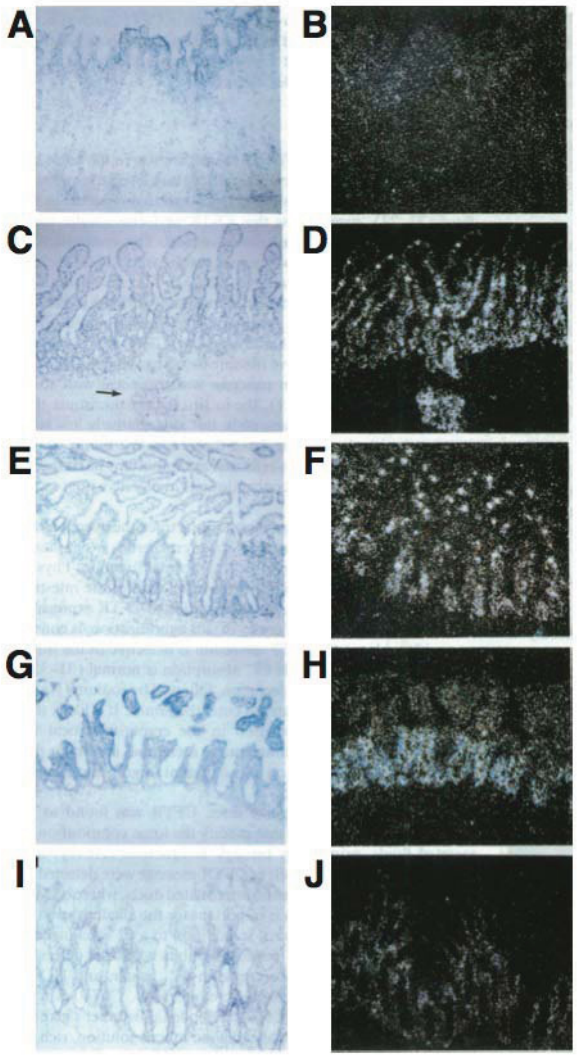

Figure 4. CFTR gene expression in the human gastrointestinal tract.
(Left) Bright field photomicrograph of tissue hybridized with an antisense probe specific for the R domain of CFTR. **(Right)** Same field visualized with dark field optics. Tissue regions are organized as follows: **(A-B)** Stomach (60X); **(C-D)** Duodenum (60X); **(E-F)** Jejunum (80X); **(G-H)** Ileum (80X); **(I-J)** Colon (80X). Generally, CFTR expression is low in the stomach and highest in the duodenum. CFTR expression decreases distally towards to colon. CFTR expression is also highest in the base of the crypts, and decreases towards villi tips. Adapted from [71].

1.4.1 Intestinal obstruction

In addition to chloride and bicarbonate secretion, CFTR regulates the function of other membrane proteins, including an epithelial sodium channel (ENaC) [75]. Together, these proteins control the movement of water and ions through the epithelium and are of critical importance for the maintenance of mucous membranes [76]. CFTR dysfunction results in dehydration of the epithelial surface and perturbed ion transport [76]. It is this altered milieu and resultant mucus accumulation that is the major cause of pathogenesis in CF intestinal disease [73].

The most serious acute complication of the CF intestinal phenotype is obstruction of the terminal ileum or proximal colon, referred to as meconium ileus (MI) [77]. This condition occurs in approximately 20% of the CF neonate population and can lead to rupture of the intestinal wall, and potentially sepsis, if left untreated [73]. Osmotic agents are frequently used as a first-line treatment for MI in an attempt to ameliorate the intestinal obstruction, termed "mucofeculant" [78, 79]. However, surgical intervention via blockade removal or intestinal resection is often required in more serious cases [73].

Intestinal obstruction due to mucus accumulation is also observed in older CF patients [79]. Similar to the incidence of MI, distal intestinal obstructive syndrome (DIOS) occurs in approximately 20% of patients and is associated with severe CF genotypes [80]. These patients are typically predisposed to constipation and present with pancreatic insufficiency comorbidity [80]. Interestingly, major intestinal mucus genes (*Muc2/Muc3*) do not have increased gene expression in CF mice despite elevated mucin glycoprotein, suggesting that CF patients have

decreased mucus clearance rather than increased synthesis [81, 82, 83]. Furthermore, an increase in mucin secretion from goblet cells is likely stimulated by bacterial overgrowth in the CF small intestine [83].

1.4.2 Bacterial colonization

The presence of small intestinal bacterial overgrowth (SIBO) has been well documented, occurring in approximately 30-40% of CF patients and murine models [84]. In particular, CF mice have a 40-fold increase in bacterial load in the small intestine when compared to WT controls [85]. Within the expanded bacterial community, there is a loss of species diversity and a predominance of Gram-negative Enterobacteriaceae [85]. Although bacteria has been observed to colonize the CF mucus, SIBO is most pronounced in the proximal small intestine and therefore not likely due to accumulation of mucofeculant material in the terminal ileum [86].

In conjunction with SIBO, the CF intestine has been shown to have a dysbiosis of the microbiota. The normal gut flora of CF patients and murine models has decreased richness, evenness, and diversity, compared to healthy controls [87]. In murine models, these microbial communities are enriched with potential pathogenic species such as *Bacteroides fragilis* and Mycobacteria species, previously associated with immunomodulation of the GI tract [87]. In particular, *B. fragilis* has been implicated in GI infection and diarrheal disease [88]. Furthermore, there is a reduced relative abundance of putative protective species including several Lactobacilliales [87].

Two potential factors in the development of SIBO have been proposed: impaired Paneth cell defenses and altered GI motility [86]. Occlusion of intestinal crypts via mucus accumulation has

been shown to reduce the movement of Paneth cell products into the intestinal lumen [85]. As a result, the antimicrobial response could be compromised and predisposed to bacterial colonization. Furthermore, the abnormal environment in the CF intestine reduces the dissolution of Paneth cell products, negatively affecting their function [89]. However, because SIBO occurs postnatal day 8 in CF mice, prior to Paneth cell development, impaired antimicrobial defenses are unlikely to be the cause of increased bacterial colonization in CF mice [86]. Therefore, the observed decrease in migrating motor complex (MMC) and gastric emptying in CF mice is the probable cause of SIBO [86].

The clinical microbiome of CF patients has yet to be fully characterized, likely due to challenges associated with high antibiotic usage [90]. However, investigation of fecal samples has provided some insight into dysbiosis in human CF populations [91]. Notably, an increased relative abundance of Bifidobacterium species and *Escherichia coli* has frequently been observed in the GI tract of children with CF [92, 93]. Although studies have had high variability in terms of other predominant microbes, it is clear that dysfunctional CFTR is permissive for intestinal dysbiosis despite lack of a CF-specific microbiome profile [90, 94].

1.4.3 Chronic inflammation

SIBO and dysbiosis of the CF intestine is believed to contribute to chronic inflammation of the small intestine, characterized by an influx of neutrophils and mast cells [81, 95]. The ΔF508 mutation causes CFTR misfolding, ER stress, and subsequent NF-κB activation, potentially augmenting the observed inflammation at steady state [96, 97]. However, mice with a complete CFTR knockout (*Cftr*$^{-/-}$) maintain an inflamed phenotype [85]. Importantly, neutrophil

infiltration and immune markers are significantly decreased in *Cftr*$^{-/-}$ mice after administration of broad-spectrum antibiotics, highlighting an important role of the gut microbiota [85].

Under basal conditions, there are 61 genes upregulated in the small intestine of *Cftr*$^{-/-}$ mice, primarily associated with the innate immune system and the acute-phase response [95]. Some of these genes, such as the leucine-rich α2 glycoprotein (Lrg), are markers for increased neutrophil recruitment [98]. Neutrophils are important members of the innate immune system, critical for anti-microbial killing via reactive oxygen species (ROS) production, degranulation, and phagocytosis [99].

1.4.4 Extraintestinal complications in CF

CFTR dysfunction has additional effects on the digestive system of the CF population. Approximately 60% of CF patients suffer from exocrine pancreatic insufficiency (EPI), reaching 85-90% with increased age [100]. The major manifestations of EPI are malabsorption and maldigestion resulting from a progressive reduction in the enzymatic capacity to digest food [100]. *CFTR*-deficient exocrine pancreata produce less digestive enzymes and are less efficient at the breakdown of luminal contents within the duodenum [101]. Patients with EPI are often administered enzymatic supplements in an attempt to alleviate the digestive process and help prevent steatoerrhea [101].

Similarly, approximately 5-15% of children with CF exhibit liver and bile duct defects [102, 103]. Fecal loss of bile acids leads to poor micelle formation and subsequent malabsorption of fat

and vitamins [102]. Together, pancreatic and liver deficiencies have important implications on patient health and augment the intestinal complications observed in CF populations.

1.4.5 Gastrointestinal malignancy

The improvement in life expectancy of CF patients has unveiled a significant increase in the prevalence of cancer associated with CFTR-expressing sites and has identified *Cftr* as a driver gene for colorectal cancer (CRC) [70, 104]. In particular, the epithelial surface of the CF small intestine and colon has increased rate of malignancies compared to controls, with risk of malignancy increasing with age [70]. These patients do not develop tumors in other CFTR-expressing tissues, such as the lung and genital tract, suggesting that malignancy development is restricted to regions with highest CFTR expression [70].

Recent studies have highlighted *Cftr* as a tumor suppressor gene and *Cftr* deficiency has been shown to cause intestinal tumors in $Cftr^{-/-}$ mice [105]. RNA-sequencing analysis of *Cftr*-deficient tumors has shown alterations in the Wnt/β-catenin signaling pathway [105]. Signaling by the Wnt family is fundamental to embryonic development and intestinal homeostasis through modulation of cell proliferation, polarity, and fate determination [106]. Efficient homeostatic renewal of the intestinal epithelium is a necessary response to both chemical and mechanical stress [106].

The most studied Wnt pathway is canonical Wnt signaling, which affects developmental gene expression through regulation of co-activator β-catenin [107]. A schematic representation of canonical Wnt signaling is outlined in Figure 5 [108]. In brief, binding of Wnt ligands to their

respective receptors releases β-catenin from the APC destruction complex [108]. The resultant cytoplasmic accumulation of β-catenin is then translocated to the nucleus and initiates transcription of Wnt target genes [108].

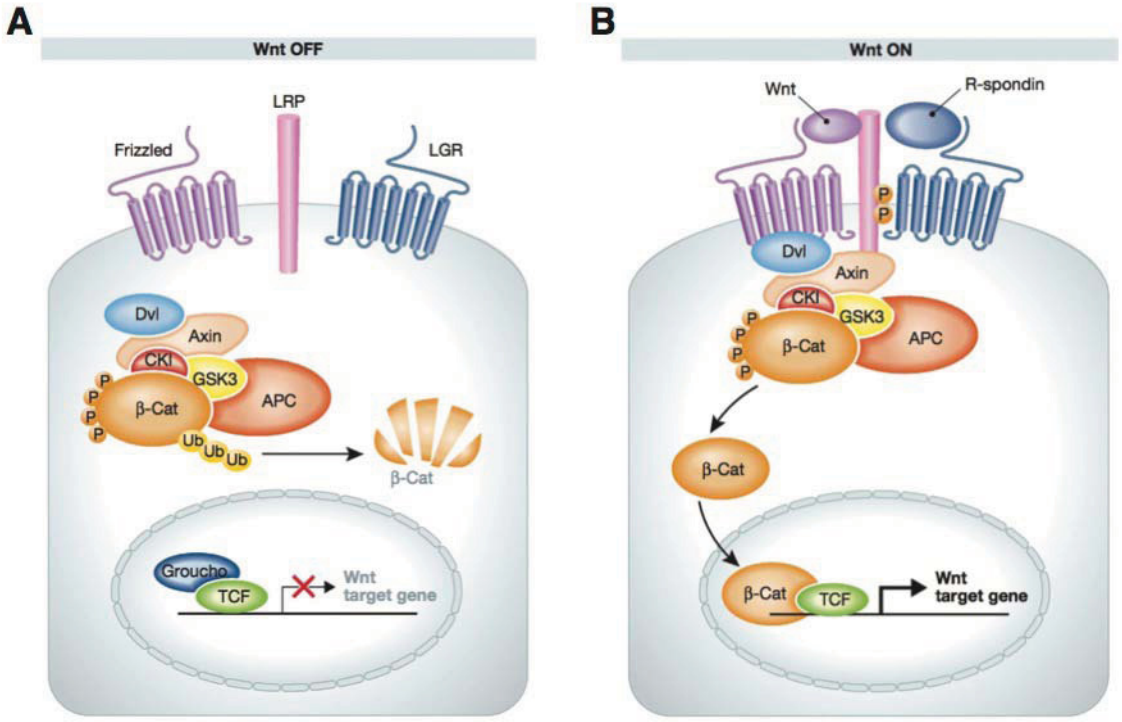

Figure 5. Canonical Wnt signaling in the intestinal epithelium.
(A) In the absence of Wnt ligands, β-catenin is maintained in the APC destruction complex and is targeted for degradation. As a result, β-catenin does not translocates to the nucleus and there is no transcription of Wnt target genes. **(B)** In the presence of Wnt ligands (Wnt, R-spondin), there is ligation of their receptors (Frizzled, LGR) and β-catenin is released from the APC destruction complex. Cytoplasmic β-catenin is translocated to the nucleus and can initiate transcription of Wnt target genes. [108]

Taken together, the emerging prevalence of gastrointestinal malignancy in CF populations reinforces the importance of understanding CFTR function in the gastrointestinal tract.

1.5 Murine models of cystic fibrosis

Current mouse models of CF were created using traditional gene targeting strategies and have greatly increased the understanding of CF intestinal biology [109, 110]. Gene targeted animal models, including complete knockouts (*Cftr*$^{-/-}$) and mice with common point mutations (ΔF508), develop MI at birth, confirming the importance of CFTR in the GI tract [109]. These mice also suffer from many of the previously mentioned intestinal complications observed in CF patients, making them a good model to study the disease. However, most current mouse models only develop a mild lung phenotype and are not ideal to study CF respiratory disease [111]. This is likely due to unknown compensatory mechanisms that stimulate other murine chloride channels in the lung [111].

Considering the abundance and tissue distribution of CF phenotypes, one difficulty with full body knockouts is dissection of phenotypic etiology [110]. Conditional knockout mice have been generated by flanking exon 10 of the *Cftr* allele with loxP sites, allowing for conditional deletion of exon 10 by directed expression of the bacterial Cre recombinase [110]. The study of cell-specific models of *Cftr* deletion will provide insight into the mechanisms and effect of CFTR disruption.

Gut-corrected CF mice have been created in order to ameliorate intestinal obstruction, a common cause of death in *Cftr*$^{-/-}$ and ΔF508 mice post-weaning [112]. A human WT *CFTR* (h*CFTR*) gene was expressed in *Cftr*$^{-/-}$ mice under the control of the rat intestinal fatty acid-binding gene promoter 2 (FABP2) [112]. FABP2 is expressed primarily in the cytosol of small intestinal epithelial cells [113]. Gut-corrected CF mice survive post-weaning and show functional

correction of goblet and crypt cell hyperplasia as well as cAMP mediated chloride secretion [112]. The small amount of h*CFTR* present in the colon is not enough to correct CFTR function in this region [112].

1.6 Enteropathogenic and enterohemorrhagic *Escherichia coli*

Enteropathogenic and enterohemorrhagic *Escherichia coli* (EPEC and EHEC) are Gram-negative attaching and effacing (A/E) pathogens associated with high morbidity and mortality [114]. Since the 1940s and 1950s, EPEC and EHEC have continued to be implicated in intestinal disease and place a major burden on human health [114, 115]. EPEC is a major cause of infantile diarrhea in developing countries, often leading to death [114]. EHEC is more prevalent in developed countries and can cause kidney failure via expression of a highly potent Shiga toxin [114].

A/E lesion formation is what distinguishes these extracellular pathogens from commensal *E. coli* strains. A/E lesion formation is characterized by intimate attachment to the intestinal epithelium and effacement of the brush border microvilli [116, 117]. Then, EPEC and EHEC use host actin polymerization machinery to form pedestal-like structures under the adherent bacterium. Bacterial virulence factors can then be injected into the host via a Type III secretion system (T3SS) [116, 117].

Disease severity and clinical outcome upon infection varies greatly between individuals, and the mechanisms that regulate susceptibility to these important pathogens remain largely unknown [118, 119].

1.6.1 Citrobacter rodentium as a model of EPEC and EHEC

Citrobacter rodentium is a widely accepted murine model of EPEC/EHEC infections in humans and is considered a "gold standard" model to study virulence mechanisms of A/E pathogens [120]. Like EPEC and EHEC, *C. rodentium* is a Gram-negative extracellular pathogen that is characterized by A/E lesion formation [121, 122]. *C. rodentium* shares approximately 67% of its genes with EPEC and EHEC, including the locus of enterocyte effacement (LEE), a pathogenicity island required for virulence [123]. The LEE encodes for a T3SS and various virulence factors which are conserved across all three pathogens [123].

C. rodentium is transmitted via the oral-fecal route, with bacteria detectable initially in the caecal patch, followed by primary colonization in the distal colon [124]. Bacterial levels peak in the distal colon between days 5 – 14 and are on the magnitude of 10^9 / g of tissue [124]. Susceptibility to *C. rodentium* is dependent on genetic background and varies between mouse strains, causing self-limiting colitis in some inbred strains (ie. C57BL/6, BALB/c) and fatal diarrhea in others (ie. C3H/HeJ, C3H/HeOuJ) [124]. Mortality of susceptible mice is a result of severe inflammation and lethal dehydration. The major clinical manifestations of *C. rodentium* infection are hyperplasia of the distal colon and immune cell influx [125, 126].

1.6.2 The host response to C. rodentium infection

The host response to intestinal infection with *C. rodentium* is a multi-faceted immune response that occurs predominantly in the intestinal lamina propria and involves several different effectors. The major cell types involved are summarized in Figure 6 [120].

In brief, the innate immune response to *C. rodentium* infection is primarily initiated through TLR2 and TLR4 signaling [127, 128]. Through the adaptor protein MyD88, TLR2 and TLR4 on epithelial and myeloid cells leads to NF-κB activation and production of IL-6, IL-12, IL-23, and tumor necrosis factor (TNF) by neutrophils, macrophages, and dendritic cells (DCs) [129, 130, 131]. These myeloid cell types, in particular neutrophils, are a critical first step in the clearance of the bacteria. These cells can also trigger a caspase 1 and IL-1 family response in a caspase 11 and NLRP3 inflammasome-dependent manner [132]. Collectively, the cytokines produced induce a pro-inflammatory response and lead to increased recruitment of both innate and adaptive immune cells.

Adaptive immune cells, including B cells and $CD4^+$ T cells, are also critical to the host response against *C. rodentium* and mice lacking these immune cells are hypersusceptible to infection [133, 134]. In particular, there is a robust Th1 and Th17 response following *C. rodentium* infection, with the Th17 response more profound [135]. Molecules involved in the differentiation and proliferation of Th17 cells, such as transforming growth factor β (TGFβ) and IL-23, are critical for the response against *C. rodentium* [135]. Furthermore, the effector molecules of Th17 cells, such as IL-17A and IL-17F, are also critical to the response that leads to increased neutrophil recruitment [135, 136]. In addition to IL-17, the production of IL-22 by certain subsets of $CD4^+$ T cells and innate lymphoid cells (ILCs) is essential for *C. rodentium* protection [137]. IL-22 production by ILC3s is especially important for the production of AMPs such as regenerating islet-derived protein 3 gamma (REGIIIγ) and beta (REGIIIβ) by IECs [137].

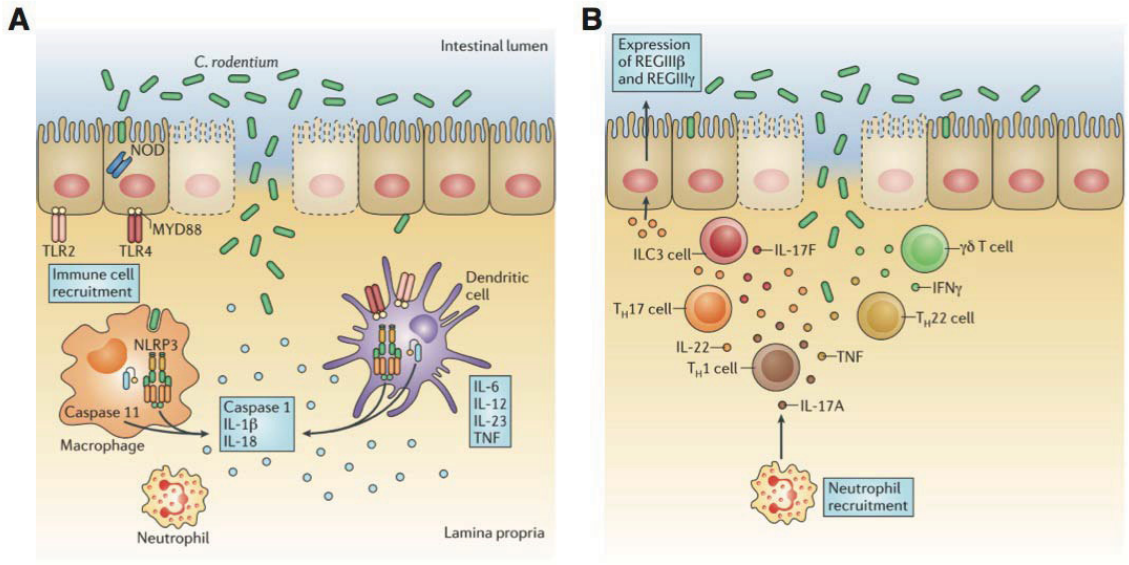

Figure 6. Host response to *Citrobacter rodentium* infection.
(A) Major innate immune response to *C. rodentium* infection: Myeloid cell recruitment primarily through TLR2 and TLR4 signaling; production of pro-inflammatory cytokines IL-6, IL-12, IL-23, TNF, Caspase 1, IL-1β, and IL-18. **(B)** Major adaptive immune response to *C. rodentium* infection: IL-17 production by Th17 cells and ILC3s leads to increased neutrophil recruitment; IL-22 production by ILC3s and other $CD4^+$ T cell subsets increases production of AMPs. [120]

1.6.3 Wnt signaling in host susceptibility to C. rodentium infection

The essential role of Wnt signaling in intestinal homeostasis has been described above. Recently, Wnt signaling has been shown to play a key role in susceptibility to *C. rodentium* infection [138]. In particular, the gene encoding for R-spondin 2 (RSPO2) is a major determinant of susceptibility to *C. rodentium* and is upregulated to high levels during infection specifically in susceptible mouse strains [138]. RSPO2, along with other members of the R-spondin family of secreted proteins, has been shown to be a potent enhancer of canonical Wnt signaling [139]. Within the GI tract, these proteins are necessary for the maintenance of intestinal stem cells and play an important role in cell fate and proliferation [140]. In susceptible mice with high RSPO2 expression, Wnt-pathway activation triggers the proliferation of immature precursors in the intestinal epithelium and inhibits the differentiation of mature IEC lineages [138]. The

undifferentiated epithelium of susceptible mice lacks proper function and fluid absorption, resulting in dehydration from diarrhea [138].

Chapter 2: Rationale and Objectives

We have found that FVB ΔF508 and BALB/c *Cftr*$^{-/-}$ mice are significantly more susceptible to *C. rodentium* infection compared to WT mice (Figure 7). FVB ΔF508 mice begin to display mortality at 7 days post-infection (DPI) and have a 14% survival rate by 12DPI. Conversely, all FVB WT mice clear the infection with a 100% survival rate through 30DPI. Similarly, less than 50% of BALB/c *Cftr*$^{-/-}$ mice survive past 12DPI, while all BALB/c WT mice survive through 30DPI. Uninfected mutant mice that survive past weaning have similar life expectancy to WT counterparts.

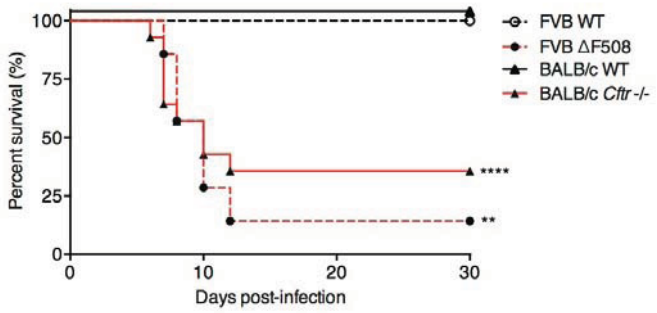

Figure 7. CF mice are significantly more susceptible to *C. rodentium* infection.
Percent survival of FVB ΔF508 (n = 7), FVB WT (n = 7), BALB/c *Cftr*$^{-/-}$ (n = 14) and BALB/c WT (n = 22) mice following oral infection with *C. rodentium*.

Therefore, **we hypothesize that CFTR plays a vital role in the host response to intestinal infection**, and that this infection model may provide insights related to CF-associated diseases. To further investigate the role of CFTR during intestinal infection, this study has the following research aims:

Aim 1 – Further characterize the defect in bacteria-host interactions in ΔF508 mice

Aim 2 – Determine the role of CFTR in hematopoietic vs. non-hematopoietic cells in intestinal infection response

Chapter 3: Materials and Methods

3.1 Ethics statement

All breeding and experimental procedures were carried out in accordance with the Canadian Council on Animal care and approved by our local ethical committee (permit #5009). Mice were euthanized by CO_2 asphyxiation and all efforts were made to minimize suffering.

3.2 Mouse breeding and infection

BALB/c.129P2-*Cftr*^{tm1Unc} (*Cftr*$^{-/-}$) and FVB/N.129P2-*Cftr*^{tm1Eur} (ΔF508) mice were generously provided by Dr. John Hanrahan (McGill University, QC). B6.129P2-*Cftr*^{tm1Unc}.FVB-Tg(FABPCFTR)1Jaw/J (Gut-corrected), B6.129P2-Lyz2$^{tm1(cre)Ifo}$/J (LysMcre), and B6.Cg-Tg(Vil1-cre)1000Gum/J (Vil1-cre) mice were obtained from The Jackson Laboratory (Bar Harbor, ME). B6.129-*Cftr*^{tm1Cwr} (*Cftr*^{fl10}) mice were obtained from Dr. Mitchell Drumm (Case Western Reserve University, OH). LysMcre *Cftr*^{fl10} mice were generated by crossing *Cftr*^{fl10} mice with the F1 progeny of LysMcre X *Cftr*^{fl10}. Presence of the LysMcre transgene and floxed *Cftr* gene was validated by PCR as previously described [42].

All mice were maintained in a specific pathogen-free facility at McGill University, provided standard mouse chow and water *ad libitum*, and transferred to Biohazard Level 2 rooms for infection. *Cftr*$^{-/-}$ and ΔF508 and their WT littermates mice were kept on polyethylene glycol in the form of CoLyte (69.5g CoLyte/L containing 60g polyethylene glycol/L) (Pendopharm) since weaning.

C. rodentium strain DBS100 was grown overnight in 3 ml of Luria-Bertani (LB) medium shaking at 37°C. Six to eight-week-old male and female mice were infected by oral gavage with 0.1 ml of LB medium containing 2-3 x 10^8 colony-forming units of bacteria. The infectious dose was confirmed by plating of serial dilutions. A bioluminescent strain of *C. rodentium* DBS100 expressing the *lux-CDABE* operon from *Photorhabdus luminescens* was obtained from Dr. Bruce Vallance (University of British Columbia, BC) [141]. For bacterial enumeration studies, a chloramphenicol-resistant derivative of *C. rodentium* DBS100 was utilized. Mice were monitored daily and euthanized on experimental days 4 and 8. Tissues for RNA isolation were dissected and snap frozen in liquid nitrogen.

3.3 Bioluminescent imaging

At 8 DPI with bioluminescent *C. rodentium*, mice were dissected to remove the lower GI tract. Tissue was imaged using a Caliper IVIS-100 (Xenogen).

3.4 Histological staining

Tissue sections were fixed in 10% buffered formalin, paraffin-embedded, sectioned at 4 μm, and either stained with hematoxylin and eosin (H&E) or left unstained. Unstained sections were deparaffinized with xylene and rehydrated through an ethanol gradient to water. Antigen retrieval was achieved by boiling sections in a 0.1M citric acid 0.1M trisodium citrate solution for 10 minutes, followed by cooling to room temperature. Sections were blocked using 10% fetal calf serum (FCS; Wisent) in PBS containing 3% bovine serum albumin (BSA; Sigma) and 0.2% Tween 20 (BioShop) for 1 hour at 37°C. Primary antibodies were diluted in PBS containing 3% BSA and 0.2% Tween 20 and incubated for 3 hours at 4°C. The primary antibodies used were

rabbit anti-*E.coli* Poly D8 LPS (1:100; Mast Group) and rabbit anti-Muc2 (1:100; Santa Cruz Biotech) followed by incubation for 1 hour at 37°C using an AlexaFluor 488-conjugated goat anti-rabbit IgG secondary antibody (1:100; Molecular Probes/Invitrogen) diluted in PBS containing 3% BSA and 0.2% Tween 20. Following application of 4', 6'-diamidino-2-phenylindole (DAPI; Sigma) for DNA staining, sections were mounted using ProLong Gold Antifade reagent (Molecular Probes/Invitrogen). Sections were imaged at 350 and 488 nm on a Zeiss Axiovert 200M microscope and images were obtained using a Hamamatsu Monochrome camera operating through AxioVision software (Version 3.0).

3.5 RNA extraction and quantitative RT-PCR

Total RNA from the proximal colon was isolated using TRIzol (Invitrogen) according to the manufacturer's instructions. The purity of RNA was assessed by a spectrophotometer; all samples had a 260/280 absorbance ratio between 1.8 and 2.0. Complementary DNA was synthesized from 1 μg of RNA with ProtoScript II reverse transcriptase (NEB) and random primers (Invitrogen) using an Eppendorf PCR thermal cycler. Expression levels of *Reg3γ* and *Reg3β* were measured using TaqMan Gene Expression Assays (Applied Biosystems) and expression levels of *KC, IFNγ, IL-1β,* and *TNFα* were measured using SYBR Green PCR Master Mix (Applied Biosystems) on a StepOnePlus Real-Time PCR system (Applied Biosystems). Analysis was performed according to the comparative C^T method using *Gapdh* as the housekeeping gene. Primer pairs for SYBR Green assays are listed in Table 1.

Table 1. SYBR Green primers for RT-qPCR		
Primer	Direction	Sequence
Ifng	F	ACTGGCAAAAGGATGGTGAC
	R	ATCCTTTTTCGCCTTGCTGT
Il1b	F	CAGGCAGGCAGTATCACTCA
	R	AGGTGCTCATGTCCTCATCC
Cxcl1 (Kc)	F	CACCTCAAGAACATCCAGAGC
	R	CTTGAGTGTGGCTATGACTTCG
Tnf	F	CATCTTCTCAAAATTCGAGTGACAA
	R	TGGGAGTAGACAAGGTACAACCC
Gapdh	F	TGCACCACCAACTGCTTAGC
	R	GGCATGGACTGTGGTCATGAG

3.6 Isolation of intestinal lamina propria cells

Intestinal lamina propria cells from mice were isolated using a modified version of a previously described method [142]. In brief, the small intestines and colons were removed and placed in cold calcium- and magnesium-free Hanks balanced salt solution (HBSS; Gibco) supplemented with 2% heat-inactivated FCS and 15 mM HEPES (Gibco). Intestines were cut open longitudinally, washed thoroughly, cut into 2 cm pieces, and incubated with shaking in EDTA buffer (HBSS supplemented with 2% FCS, 15 mM HEPES, and 5 mM EDTA) for 60 minutes at 37°C to remove epithelial cells. After removing the supernatant, tissue pieces were incubated in RPMI-1640 (Sigma) supplemented with 10% FCS, 15 mM HEPES, 100 μg/ml DNase I (Roche) and 200 μg/ml collagenase type IV (Sigma) for 40 minutes at 37°C. Cell suspension was filtered through a 70 μm cell strainer (Sigma), washed, and resuspended in FACS buffer (1X PBS supplemented with 2% FBS and 0.5M NA_2EDTA) before proceeding with antibody staining.

3.7 Isolation of mouse bone marrow cells

Bones from mouse hind legs (tibia and femur) were dissected, removed of excess fat and muscle, and placed in cold RPMI-1640 supplemented with 10% FCS and penicillin streptomycin

(Wisent). Bone marrow was flushed with RPMI-1640 supplemented with 10% FCS, penicillin streptomycin and 2 mM EDTA using a 25G -5/8" needle and passed through a 70 μm cell strainer. RBC lysis was performed by adding 2ml of 1X ACK RBC lysis buffer (0.15M NH_4Cl, 10mM $KHCO_3$, 1mM NA_2EDTA) for 2 minutes. Cells were washed and resuspended in FACS buffer before proceeding with antibody staining.

3.8 Oxidative burst assay

Five million cells were incubated in 1:3000 dihydrorhodamine 123 (10 μM) (DHR; Life Technologies) in RPMI-1640 supplemented with 10% FCS and penicillin streptomycin for 5 minutes at 37°C with 5% CO_2. Phorbol 12-myristate 13-acetate (PMA; Sigma) was added 1:16000 (100 nM) in RPMI-1640 supplemented with 10% FCS and penicillin streptomycin and incubated for 25 minutes at 37°C with 5% CO_2. Cells were placed on ice for 2 – 3 minutes before transfer to FACS tubes for antibody staining.

3.9 Flow cytometry

Cells were incubated with 1 mg/ml rat anti- mouse CD16/CD32 Ab (Fc-block; clone 2.4G2) for 15 min at 4°C and then washed with cold FACS buffer. Fluorochrome-labeled extracellular antibodies were added in a total volume of 100 μl, mixed thoroughly, and incubated for 25 minutes at 4°C. Extracellular antibodies used in this study are listed in Table 2 and were used at a dilution of 1:200. All antibodies, except for Siglec-F (BD Pharmingen) and β-catenin (Cell Signaling), were purchased from eBioscience. Following extracellular staining, cells were washed with PBS and resuspended in viability dye (Life Technologies) for 20 minutes at 4°C. Intracellular staining for IFNγ (XMG1.2; eBioscience), IL-17 (eBio17B7; eBioscience), IL-22

(1H8PWSR; eBioscience), and RORγτ (B2D; eBioscience) was performed using the FoxP3 transcription factor staining buffer kit (eBioscience) and antibodies were used at a dilution of 1:100. Prior to staining, cells were stimulated with Cell Stimulation Cocktail (plus protein transport inhibitors) (eBioscience) for 3 hours at 37°C. Annexin-V staining was performed using the Annexin V apoptosis detection kit (eBioscience). A FACSCanto II (BD Biosciences) was used for immunophenotyping, oxidative burst, and Annexin-V panels. For confirmation of *Cftr* excision in LysMcre $Cftr^{fl10}$ mice, cells were purified using various methods. Splenic T cells were purified using a $CD8a^+$ Isolation Kit (Miltenyi Biotech). Neutrophils from the bone marrow were isolated using density gradient centrifugation and Histopaque 1077 and 1119 (Sigma). Lastly, bone marrow was cultured for 5 days in RPMI-1640 supplemented with 10% FCS and 30% macrophage colony stimulating factor (MCSF; L929 cells) at 37°C with 5% CO_2 to get bone marrow derived macrophages (BMDMs). Cell purity was confirmed on a FACSCanto II.

Table 2. Extracellular antibodies used for flow cytometry

Antibody	Conjugate	Clone
β-catenin	PE	D13A1
CD3	PerCP-Cy5.5	145-2C11
CD4	PE.Cy7	GK1.5
CD8a	FITC	53-6.7
CD11b	eF450	M1/70
CD11c	FITC	N418
CD19	PerCP-Cy5.5	eBio1D3
CD45	APC.Cy7	30-F11
CD54 (ICAM-1)	FITC	YN1/1.7.4
F4/80	PE.Cy7	BM8
Ly6C	APC	HK1.4
Ly6G	PerCP-Cy5.5	RB6-8C5
NKp46	eF450	29A1.4
Siglec-F	PE	E50-2440
TCRβ	PerCP-Cy5.5	H57-597
TCRγδ	eF450	eBioGL3
TER-119	PerCP-Cy5.5	TER-119

3.10 Intravascular staining

Each mouse was injected with 300 µl of antibody dilution (2 µg CD45-FITC in PBS) intravenously via the tail vein. After 3 minutes, each mouse was anaesthetized by isoflurane and a blood sample collected by retro-orbital bleeding. Following cervical dislocation, the GI tract was dissected and the intestinal lamina propria isolated as described previously. Extracellular staining was performed ex vivo, including CD45 in another fluorochrome (APC-Cy7).

3.11 Statistics

Survival curves were analyzed using a Log-rank test. Other data analyses were performed using the Mann-Whitney test. All analyses were performed on GraphPad Prism software (Version 6.0). *$p<0.05$; **$p<0.01$; ***$p<0.001$, ****$p<0.0001$

Chapter 4: Results

4.1 Altered localization and greater colonization of *C. rodentium* in ΔF508 mice

ΔF508 mice are significantly more susceptible to *C. rodentium* infection compared to WT mice, with almost 100% mortality. To further examine the susceptibility of *Cftr* mutant mice, ΔF508 and WT mice were infected with a bioluminescent strain of *C. rodentium* and their gastrointestinal tracts visualized using an *in vivo* imaging system (IVIS) (Figure 8A). *C. rodentium* exhibited localization to the jejunum, cecum, and proximal colon at 8DPI in the ΔF508 mice. This result was atypical as *C. rodentium* usually localizes to the distal colon specifically during peak infection in susceptible mouse strains (such as C3H/HeOuJ). Conversely, WT mice had no detectable luminescent signal.

The altered localization of *C. rodentium* during peak infection was validated via immunohistochemistry (Figure 8B). At 8DPI, staining with an antibody for *C. rodentium* lipopolysaccharide (LPS) identified the interaction of *C. rodentium* with the epithelial surface of the proximal colon and cecum of ΔF508 mice. In contrast, LPS staining was not detectable in equivalent tissue sections from WT mice. Staining of serial sections with an antibody for MUC2, a major structural component of intestinal mucin, allowed for a visual analysis of the bacteria/mucus interface. Increased mucus levels were confirmed in the ΔF508 mice and its location appeared to partially correspond with that of the luminal bacteria

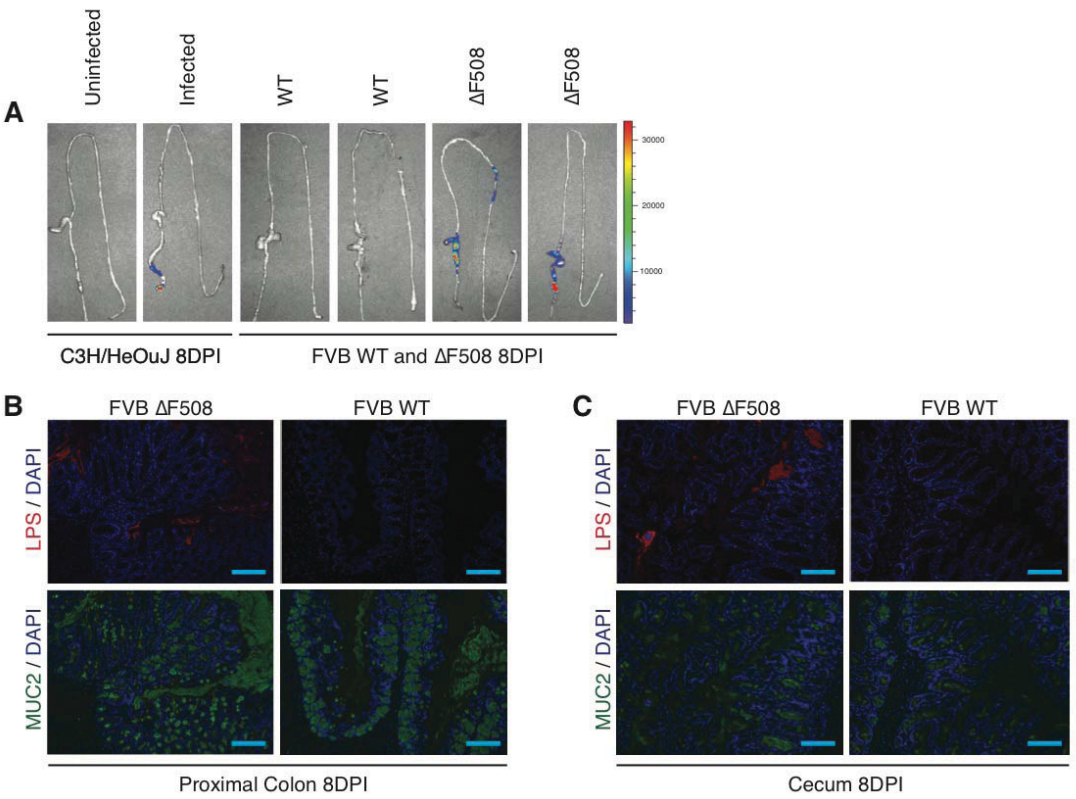

Figure 8. *C. rodentium* has an altered location in ΔF508 mice.
(A) In-vivo imaging of FVB ΔF508, FVB WT, and C3H/HeOuj susceptible mice at 8DPI with a luciferase-expressing strain of *C. rodentium*. LPS (red) and MUC2 (green) immunostained / DAPI co-stained (blue) **(B)** proximal colon and **(C)** serial sections of FVB WT and ΔF508 mice at 8DPI with *C. rodentium*. Scale bars are 100 micron.

Based on this data, the bacterial burden in various tissues of ΔF508 and WT mice was determined at 4DPI (Figure 9). In the jejunum, cecum, proximal colon, distal colon, and feces, there was a significantly higher bacterial burden in ΔF508 mice compared to WT. There were also significantly higher loads in the spleens of ΔF508 mice, indicating the systemic dissemination of *C. rodentium*.

4.2 Greater tissue response to *C. rodentium* infection in ΔF508 mice

There was a greater tissue response to *C. rodentium* infection in ΔF508 mice compared to WT. H&E staining at 8DPI showed markedly higher tissue hyperplasia and immune cell infiltration in the jejunum, cecum, and proximal colon of ΔF508 mice (Figures 10A; 10C; 10E). Conversely, minimal differences were observed between uninfected WT and ΔF508 tissues (Appendix 1). Tissue sections from the proximal colon and cecum of infected mice scored significantly higher on measures of goblet cell depletion, surface epithelial injury, edema, and immune cell infiltration as determined by a veterinary pathologist (Figures 10D; 10F). Although not significant, tissue sections from the jejunum of ΔF508 mice showed a trend towards increased histopathological score (Figure 10B). In order to examine the phenotypic differences between ΔF508 and WT mice within a longer timeframe, we infected the mice with an attenuated strain of *C. rodentium* (Δ*espF*), allowing us to continue the infection up to 13 days. In this case, we observed a prominent hyperplastic thickening of the proximal colon of ΔF508 mice that was not observed in WT mice (Figure 10G).

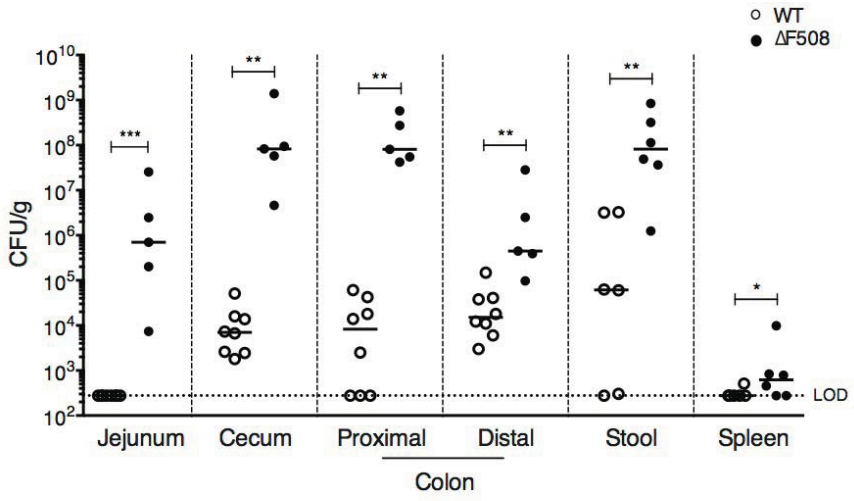

Figure 9. *C. rodentium* colonizes to a higher level in ΔF508 mice.
Bacterial burden in various tissues of FVB WT and ΔF508 mice at 4DPI with *C. rodentium* ($n \geq 5$ for all conditions). Line represents the median.

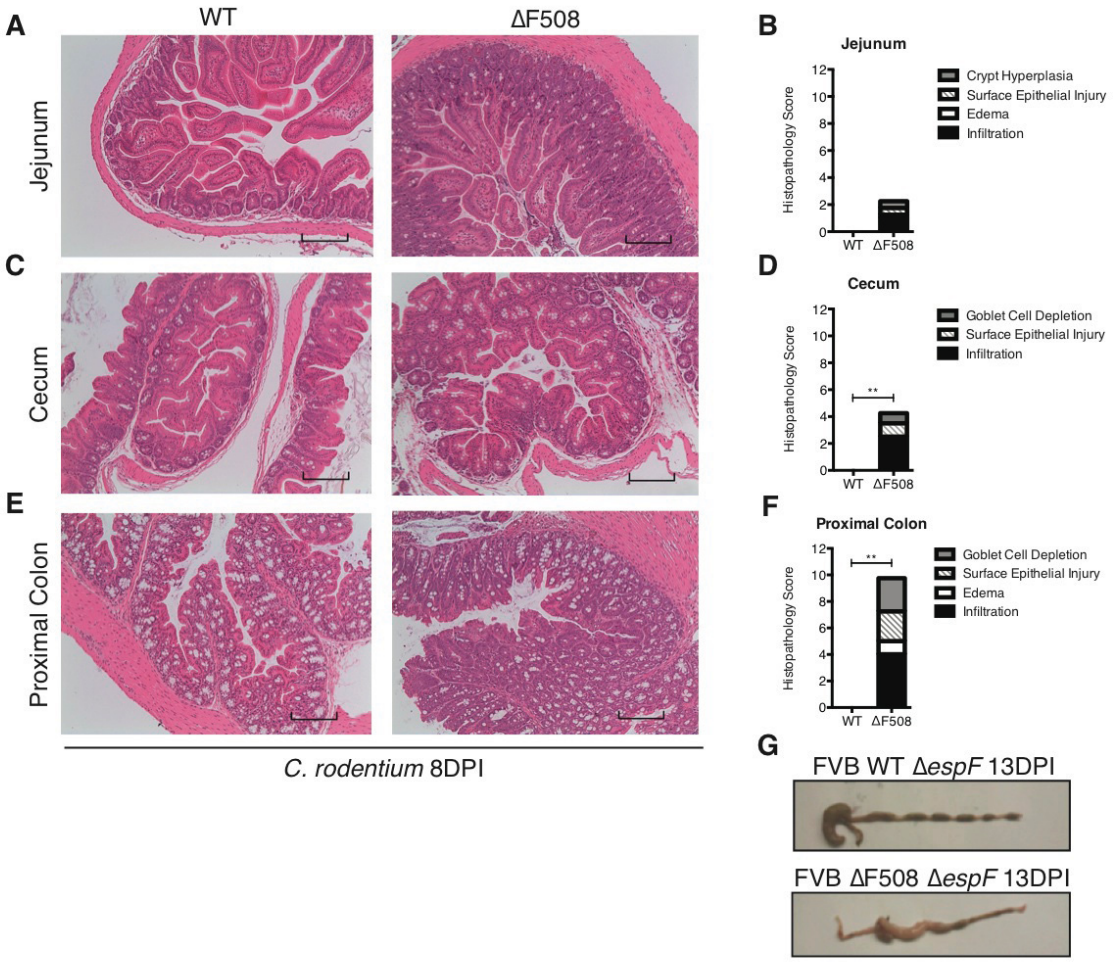

Figure 10. Greater tissue response to *C. rodentium* in ΔF508 mice.
H&E stain of **(A)** jejunum, **(C)** cecum and **(E)** proximal colon tissues of WT and ΔF508 mice at 8DPI with *C. rodentium* (10X magnification). Scale bars are 300 micron. Histopathology scoring of **(B)** jejunum, **(D)** cecum, and **(F)** proximal colon tissue sections from WT and ΔF508 mice at 8DPI with *C. rodentium* (WT $n = 4$, ΔF508 $n = 4$). **(G)** Macroscopic imaging of the large intestine of FVB WT and ΔF508 mice at 13DPI with Δ*espF C. rodentium*.

We found that following infection of ΔF508 mice, the greatest tissue response is in the proximal colon, corresponding to the tissue with the greatest bacterial burden. As such, differences in inflammatory mediator expression in the proximal colon were investigated between the two groups of mice by RT-qPCR (Figure 11A). There were significantly higher expression levels of IL-1β, CXCL1 (KC), Reg3β and Reg3γ in the proximal colon of ΔF508 mice than WT littermate mice at 4DPI with *C. rodentium*. Furthermore, there was a trend towards increased IFNγ and TNFα in ΔF508 mice compared to WT littermates.

To further characterize the inflammatory status of ΔF508 and WT mice after infection, evaluation of immune cell populations in the colon and small intestine lamina propria was performed. In both the small intestine and colon of ΔF508 mice at 4DPI with *C. rodentium*, there was significantly higher frequency and total number of $CD11b^{+}$ $Ly6G^{+}$ neutrophils compared to WT mice (Figures 11C; 11D). Similarly, there were significantly higher frequency and total number of $CD11b^{+}$ $Ly6C^{hi}$ monocytes in the colon of ΔF508 mice at 4DPI (Figure 11F). There were no significant differences observed in frequency or total number of T cells, B cells, and other myeloid subsets between ΔF508 and WT mice at 4DPI with *C. rodentium* (Appendices 1; 2).

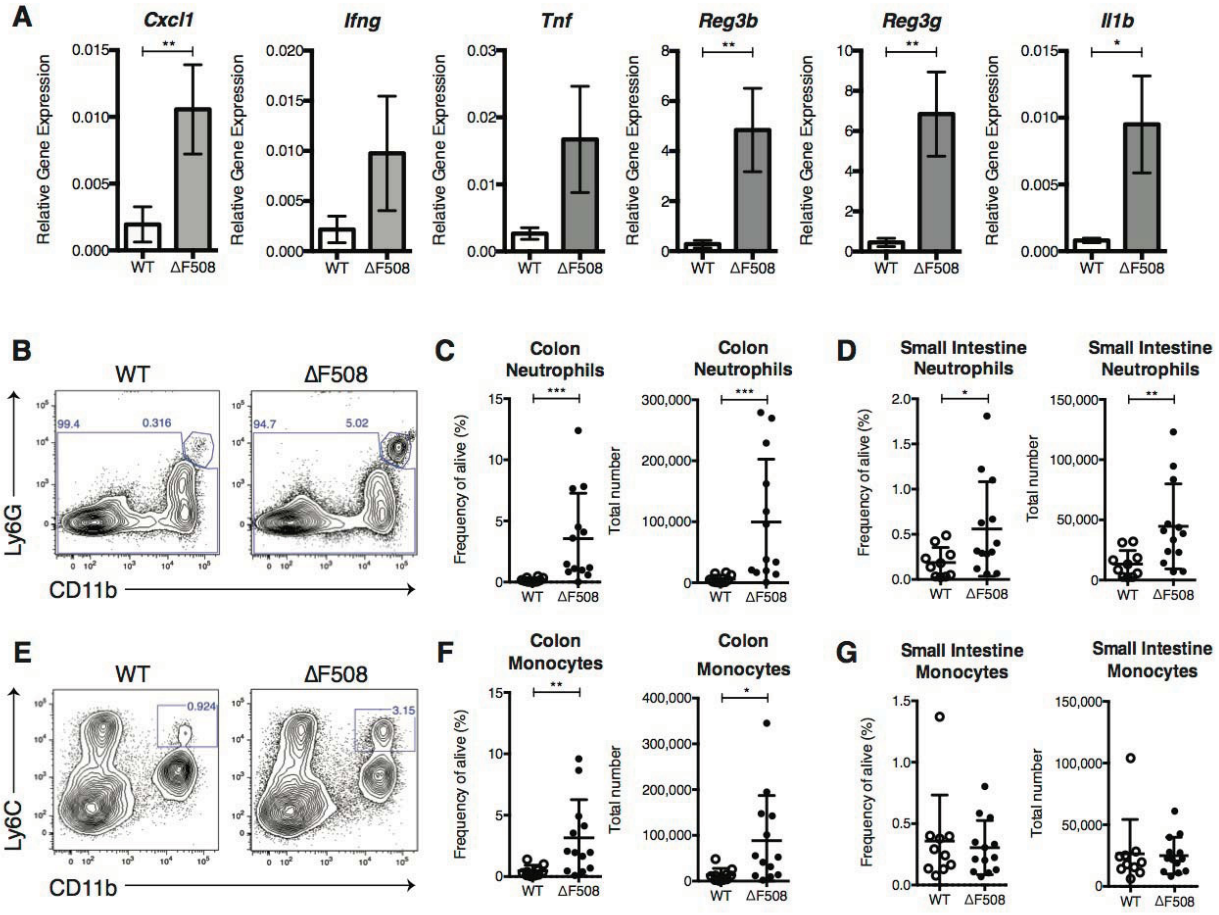

Figure 11. Increased inflammatory cytokine profile and immune cell infiltration in ΔF508 mice after infection with *C. rodentium*.
(A) Gene expression relative to GAPDH in the proximal colon of WT and ΔF508 mice at 4DPI with *C. rodentium* (WT $n = 4$, ΔF508 $n = 5$). Values displayed as mean with standard error (SEM). **(B)** Representative contour plot of $CD11b^+$ $Ly6G^+$ neutrophils in the colon lamina propria. Gated on single cells, live cells, $CD45^+$. Frequency and total number of $CD11b^+$ $Ly6G^+$ neutrophils in the **(C)** colon and **(D)** small intestine of WT and ΔF508 mice at 4DPI with *C. rodentium* (WT $n = 10$, ΔF508 $n = 13$). **(E)** Representative contour plot of $CD11b^+$ $Ly6C^{hi}$ monocytes in the colon lamina propria. Gated on single cells, live cells, $CD45^+$. Frequency and total number of $CD11b^+$ $Ly6C^{hi}$ monocytes in the **(F)** colon and **(G)** small intestine of WT and ΔF508 mice at 4DPI with *C. rodentium* (WT $n = 10$, ΔF508 $n = 13$). Values displayed as mean with standard deviation (SD).

We further investigated the origin of the increased myeloid cells in ΔF508 mice using intravascular staining. Injection of CD45-FITC intravenously (*i.v.*) via the tail vein immediately prior to euthanization, in conjunction with CD45-APC.Cy7 staining *ex vivo* after gut preparation allowed for distinction between tissue and blood neutrophils (Figure 12A). For both the small intestine and the colon, of the total neutrophils and monocytes present, the majority were in the lamina propria tissue and not stuck within the vasculature. However, it is notable that both tissue and blood neutrophils were significantly elevated in the ΔF508 mice at 4DPI with *C. rodentium* compared to WT (Figures 12C; 12F). Similarly, both tissue and blood monocytes were elevated in the ΔF508 mice (Figures 12D; 12G). Blood controls for each mouse stained ≥ 95% $FITC^+$, indicating successful IV injection and circulation.

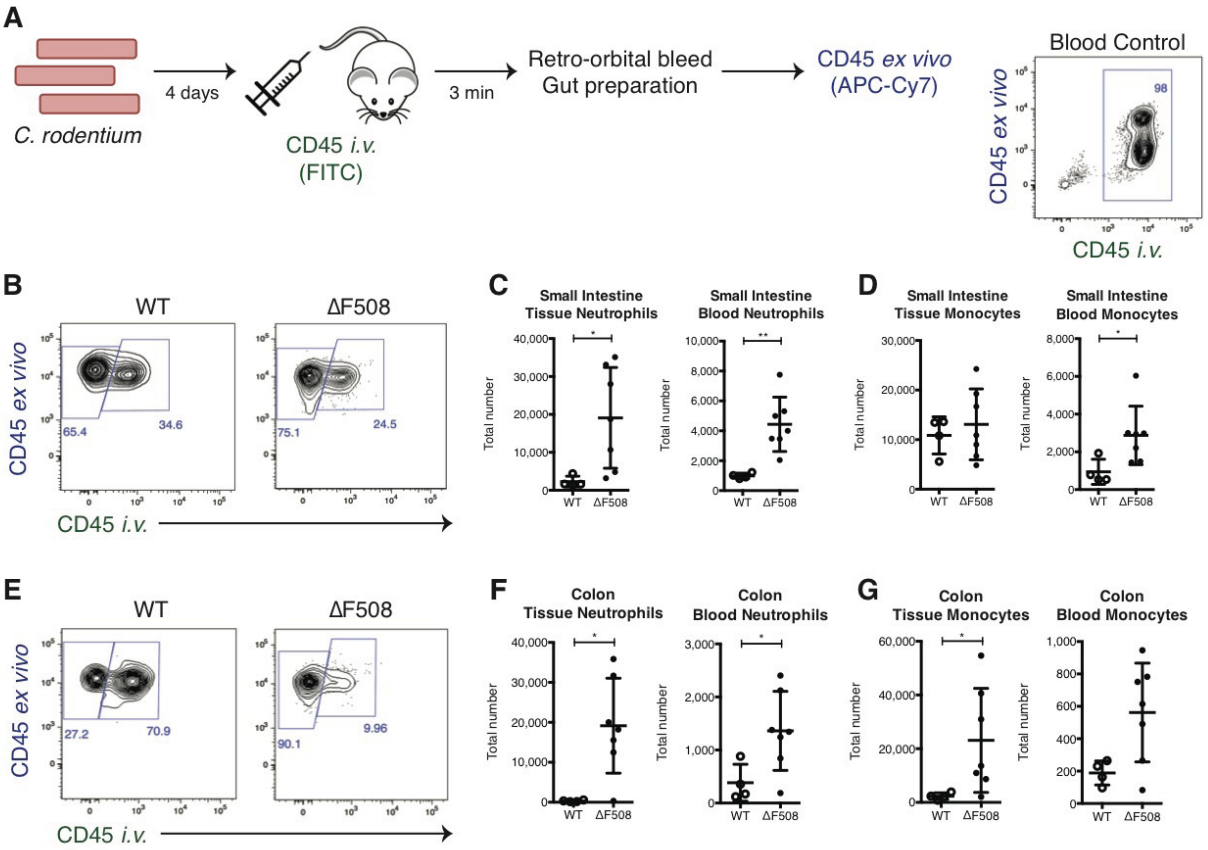

Figure 12. Infiltrating neutrophils in ΔF508 mice after *C. rodentium* infection are primarily in the tissue, as opposed to the vasculature.
(A) Experimental design and representative blood control. **(B)** Representative contour plot of $CD11b^+$ $Ly6G^+$ neutrophils in the small intestine of both WT and ΔF508 mice. Gated on single cells, live cells, $CD45^+$, $CD11b^+$, $Ly6G^+$. Total number of tissue and blood **(C)** neutrophils and **(D)** monocytes in the small intestine of WT (n = 4) and ΔF508 (n = 7) mice at 4DPI with *C. rodentium*. **(E)** Representative contour plot of $CD11b^+$ $Ly6G^+$ neutrophils in the colon of both WT and ΔF508 mice. Gated on single cells, live cells, $CD45^+$, $CD11b^+$, $Ly6G^+$. Total number of tissue and blood **(F)** neutrophils and **(G)** monocytes in the colon of WT (n = 4) and ΔF508 (n = 7) mice at 4DPI with *C. rodentium*. Values displayed as mean with standard deviation (SD).

4.3 The GI tract of ΔF508 mice is inflamed at steady state

To further examine the immune response in ΔF508 mice, in particular the role of neutrophils, their status at steady state was examined. Prior to infection, the small intestine lamina propria of ΔF508 mice had significantly higher frequency and total number of $CD11b^+$ $Ly6G^+$ neutrophils compared to WT mice (Figure 13B). Furthermore, a significantly higher total number of $CD11b^+$ $Ly6C^{hi}$ monocytes were observed in the small intestine of ΔF508 mice at steady state (Figure 13E). Although no differences in neutrophil numbers were observed (Figure 13C), there were significantly higher frequency and total number of $CD11b^+$ $Ly6C^{hi}$ monocytes in the colon of ΔF508 mice at steady state (Figure 13F). There were no significant differences observed in frequency or total number of T cells, B cells, and other myeloid subsets between ΔF508 and WT mice (Appendices 3; 4).

We also observed a significant increase in both frequency and total number of IL-17 producing Th17 cells in both the small intestine and colon of ΔF508 mice compared to WT (Figures 13E; 13F). Taken together, the majority of steady state differences in immune cell responses between ΔF508 and WT mice are more dramatic in the small intestine lamina propria as opposed to the colon.

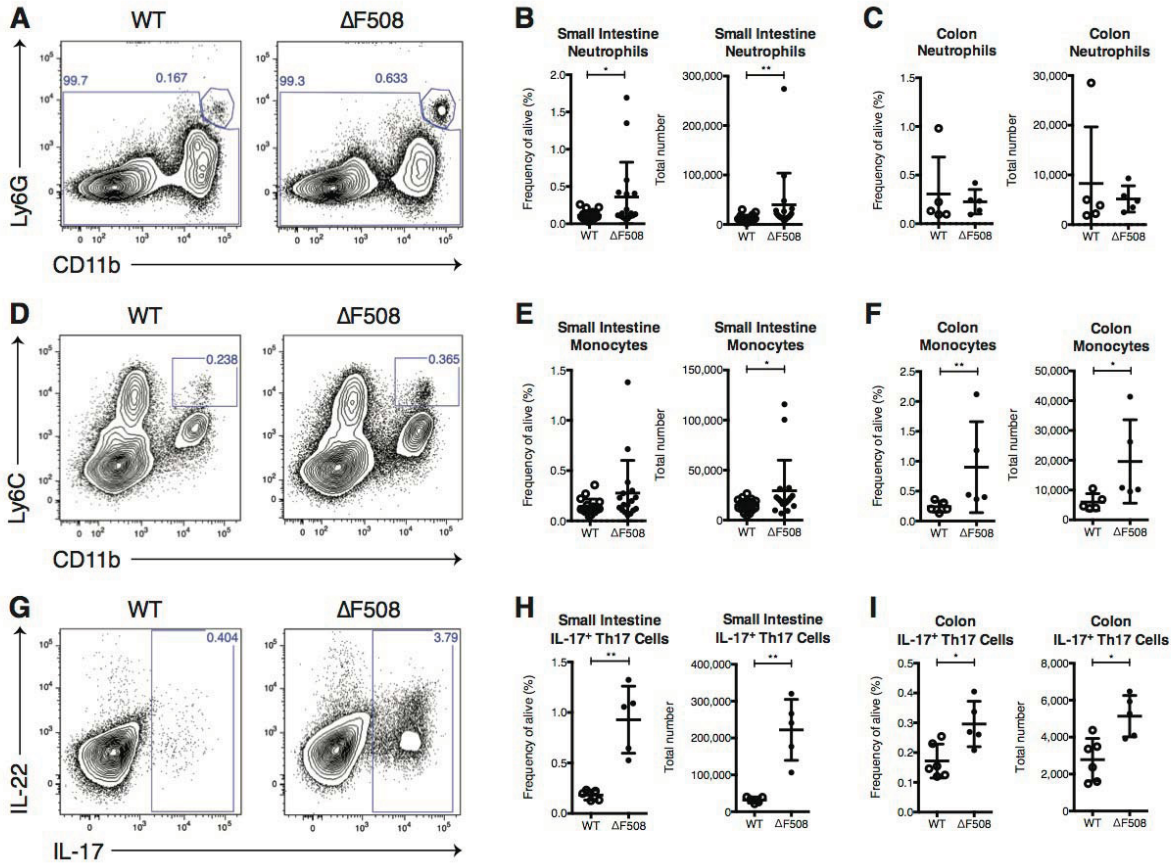

Figure 13. The GI tract of ΔF508 mice is inflamed at steady state.
(A) Representative contour plot of $CD11b^+$ $Ly6G^+$ neutrophils in the small intestine of WT and ΔF508 mice at steady state. Gated on single cells, live cells, $CD45^+$. **(B)** Frequency and total number of $CD11b^+$ $Ly6G^+$ neutrophils of the small intestine from WT (n = 18) and ΔF508 (n = 17) mice at steady state. **(C)** Frequency and total number of $CD11b^+$ $Ly6G^+$ neutrophils of the colon from WT (n = 5) and ΔF508 (n = 5) mice at steady state. **(D)** Representative contour plot of $CD11b^+$ $Ly6C^{hi}$ monocytes in the small intestine of WT and ΔF508 mice at steady state. Gated on single cells, live cells, $CD45^+$. **(E)** Frequency and total number of $CD11b^+$ $Ly6C^{hi}$ monocytes of the small intestine from WT (n = 18) and ΔF508 (n = 17) mice at steady state. **(F)** Frequency and total number of $CD11b^+$ $Ly6C^{hi}$ monocytes of the colon from WT (n = 5) and ΔF508 (n = 5) mice at steady state. **(G)** Representative contour plot of IL-17^+ Th17 cells in the small intestine of WT and ΔF508 mice at steady state. Gated on single cells, live cells, $CD45^+$, $TCR\beta^+$, $CD4^+$. **(H)** Frequency and total number of IL-17^+ Th17 cells of the small intestine from WT (n = 5) and ΔF508 (n = 5) mice at steady state. **(I)** Frequency and total number of IL-17^+ Th17 cells of the colon from WT (n = 6) and ΔF508 (n = 5) mice at steady state. Values displayed as mean with standard deviation (SD).

4.4 ΔF508 myeloid cells are deficient in ROS production

Despite an increase in myeloid immune cells both at steady state and following infection, ΔF508 mice remain highly susceptible to *C. rodentium*. Typically, an influx of neutrophils and a potent Th17 response would be considered protective against *C. rodentium* infection [129, 135]. To address the functionality of the cells present, an oxidative burst assay was performed to assess ROS production of the myeloid cells at steady state. Following stimulation with PMA, $CD11b^+$ $Ly6G^+$ neutrophils and $CD11b^+$ $Ly6C^{hi}$ monocytes from the small intestine of ΔF508 mice produced significantly less ROS compared to WT, measured as decreased oxidation of DHR to rhodamine-123 (Figure 14B). This deficiency in ROS production highlights a potential reason that the immune system in ΔF508 mice is unable to clear the infection despite elevated numbers of innate immune cells present.

To further address the functionality and activation status of ΔF508 myeloid cells, we assessed their expression of ICAM-1, an activation marker of epithelial cells and various leukocytes [142]. Preliminary results indicate that ΔF508 monocytes in the small intestine have a significantly decreased ICAM-1 expression at steady state compared to WT cells (Figure 14C). Although not significant, ΔF508 neutrophils also have a trend towards decreased ICAM-1 expression (Figure 14C). Taken together with the DHR data, these results suggest that the ΔF508 myeloid compartment is less active and has decreased ROS production at steady state.

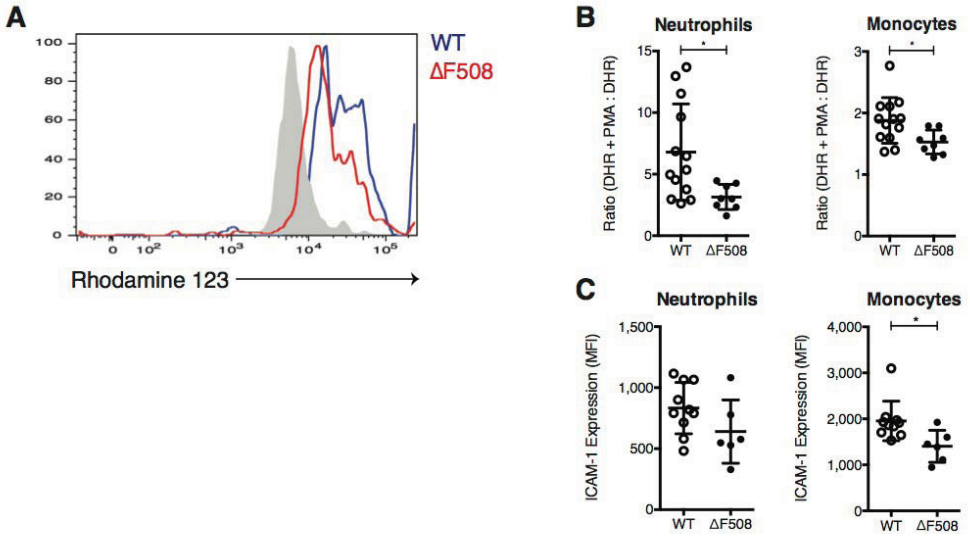

Figure 14. ΔF508 myeloid cells are deficient in ROS production at steady state.
(A) Representative histogram of Rhodamine 123 signal following the stimulation of neutrophils from the small intestine lamina propria with PMA. Gated on single cells, live cells, $CD45^{+}$, $CD11b^{+}$, $Ly6G^{+}$. **(B)** Oxidative burst activity of steady state $CD11b^{+}$ $Ly6G^{+}$ neutrophils and $CD11b^{+}$ $Ly6C^{hi}$ monocytes from the small intestine of WT and ΔF508 mice (WT $n = 13$, ΔF508 $n = 8$). **(C)** ICAM-1 expression of steady state $CD11b^{+}$ $Ly6G^{+}$ neutrophils and $CD11b^{+}$ $Ly6C^{hi}$ monocytes from the small intestine of WT and ΔF508 mice (WT $n = 10$, ΔF508 $n = 6$). Values displayed as mean with standard deviation (SD).

4.5 ΔF508 myeloid cells have decreased apoptosis compared to WT

The turnover of myeloid cells via apoptosis, deficient in the CF lung [38], is a critical step in mounting an effective immune response against infection. Therefore, the frequency of myeloid cells undergoing apoptosis in our model was addressed by Annexin-V staining. At both steady state and 4DPI with *C. rodentium*, the frequency of Annexin-V^+ $CD11b^+$ $Ly6G^+$ neutrophils and Annexin-V^+ $CD11b^+$ $Ly6C^{hi}$ monocytes from the small intestine of ΔF508 mice was significantly less than WT (Figures 15B; 15C). Overall, our data suggests that not only are the neutrophils and monocytes of the ΔF508 small intestine lamina propria deficient in ROS production, but they have decreased apoptosis and persist longer in the tissue compared to WT cells.

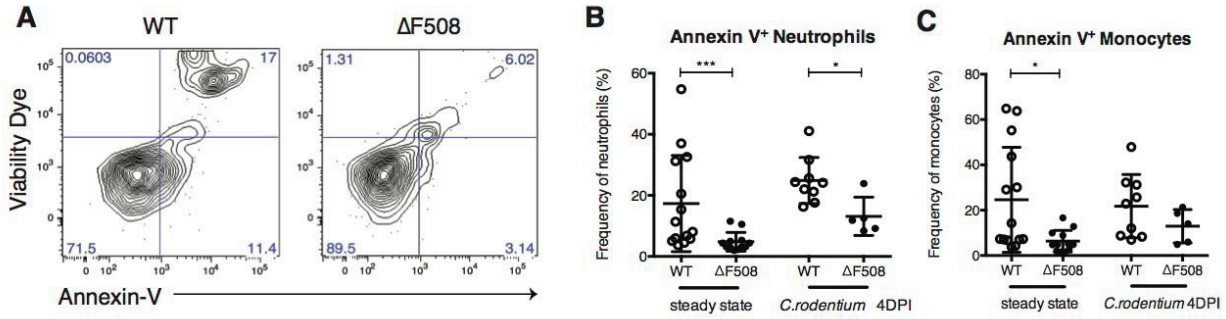

Figure 15. ΔF508 myeloid cells have decreased apoptosis compared to WT.
(A) Representative contour plot indicating Annexin-V^{+} neutrophils from the small intestine lamina propria. Gated on single cells, live cells, CD45^{+}, CD11b^{+}, Ly6G^{+}. Annexin-V staining of **(B)** CD11b^{+} Ly6G^{+} neutrophils and **(C)** CD11b^{+} Ly6C^{hi} monocytes from the small intestine of FVB WT and ΔF508 mice both at steady state (WT *n* = 14, ΔF508 *n* = 12) and 4DPI with *C. rodentium* (WT *n* = 9, ΔF508 *n* = 5). Values displayed as mean with standard deviation (SD).

4.6 Myeloid deficiencies in ΔF508 mice are not restricted to the small intestine lamina propria

Deficiencies in ROS production and apoptosis in myeloid cells of ΔF508 mice were also investigated in the bone marrow. As opposed to the small intestine, no significant differences in frequency of Annexin-V^+ $CD11b^+$ $Ly6G^+$ neutrophils and Annexin-V^+ $CD11b^+$ $Ly6C^{hi}$ monocytes were observed between ΔF508 and WT mice in the bone marrow (Figures 16C; 16D). However, similar to the small intestine, $CD11b^+$ $Ly6G^+$ neutrophils in the bone marrow of ΔF508 mice produced significantly less ROS compared to WT cells (Figure 16A). No significant differences were observed in the oxidative burst of $CD11b^+$ $Ly6C^{hi}$ monocytes in the bone marrow (Figure 16B).

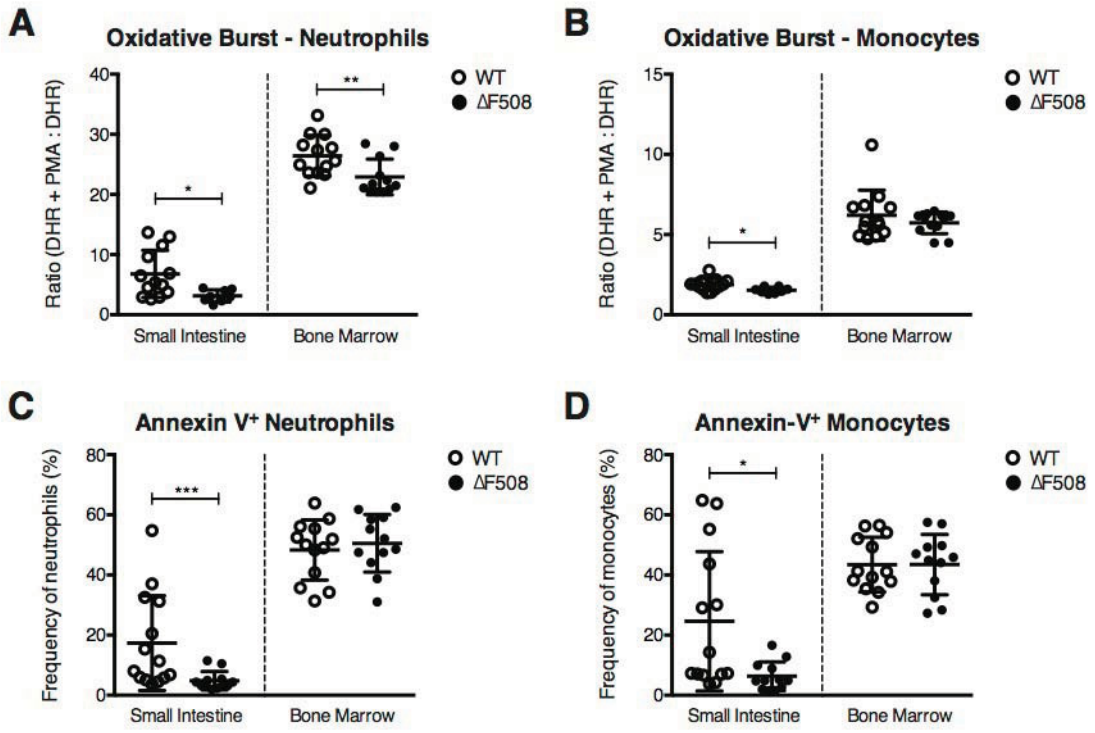

Figure 16. ΔF508 myeloid cell deficiencies are not restricted to the small intestine lamina propria. Oxidative burst activity of steady state **(A)** $CD11b^{+}$ $Ly6G^{+}$ neutrophils and **(B)** $CD11b^{+}$ $Ly6C^{hi}$ monocytes from the small intestine (WT n = 13, ΔF508 n = 8) and bone marrow (WT n = 13, ΔF508 n = 12) of WT and ΔF508 mice. Annexin-V staining of **(C)** $CD11b^{+}$ $Ly6G^{+}$ neutrophils and **(D)** $CD11b^{+}$ $Ly6C^{hi}$ monocytes from the small intestine (WT n = 14, ΔF508 n = 12) and bone marrow (WT n = 13, ΔF508 n = 12) of WT and ΔF508 mice at steady state. Values displayed as mean with standard deviation (SD).

4.7 Myeloid-specific *Cftr*$^{-/-}$ mice are resistant to *C. rodentium* infection

Deficiencies in ROS production and decreased apoptosis of ΔF508 neutrophils and monocytes warranted investigation into the role of CFTR in the myeloid compartment. To determine the relative contribution of the CFTR-deficient myeloid compartment to intestinal infection susceptibility, mice with myeloid-specific *Cftr* inactivation (LysMcre *Cftr*^{fl10}) were generated. Cre recombinase expression under the Lyz2 promoter, expressed in monocytes, mature macrophages, and granulocytes, allows the excision of *Cftr* specifically within myeloid cell types.

Cftr was present in both cell types in mice without the LysMcre transgene. Following *C. rodentium* infection, both LysMcre *Cftr*^{fl10} and WT mice had 100% survival, with no significant differences in body weight or fecal CFU (Figures 17A; 17C; 17D). No significant differences in myeloid cell oxidative burst activity (Figure 18B) or apoptosis (Figure 18D) were observed in the small intestine of LysMcre *Cftr*^{fl10} and WT mice at steady state. To confirm *Cftr* excision in mice carrying the LysMcre transgene, both myeloid and lymphoid cells were enriched from the bone marrow and spleen and DNA was extracted. As expected, *Cftr* was present in lymphoid cells, but absent from the myeloid compartment (Figure 17B). Taken together, these results suggest that the defects observed in the myeloid compartment and the susceptibility of CF mice to infection with *C. rodentium* are not due to loss of CFTR in the myeloid compartment.

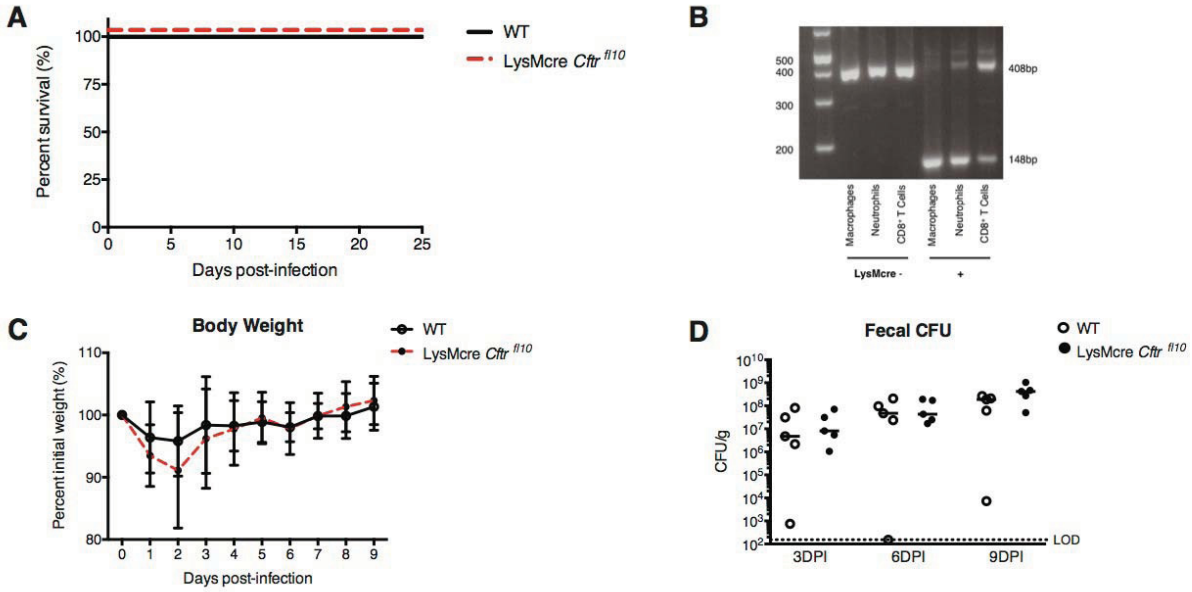

Figure 17. Myeloid-specific *Cftr*$^{-/-}$ mice are resistant to *C. rodentium* infection.
(A) Percent survival of LysMcre CFTR^{fl10} (n = 13) and WT (n = 10) mice following oral infection with *C. rodentium*. **(B)** DNA gel showing excision of CFTR from macrophages and neutrophils from the bone marrow of LysMcre CFTR^{fl10}. CFTR is present in splenic CD8^{+} T cells. **(C)** Percent initial body weight of WT (n = 5) and LysMcre CFTR^{fl10} (n = 5) mice following infection with *C. rodentium*. Values displayed as mean with standard deviation (SD). **(D)** CFU/g feces for WT (n = 5) and LysMcre CFTR^{fl10} (n = 5) mice at 3DPI, 6DPI, and 9DPI with *C. rodentium*. Line represents the median value.

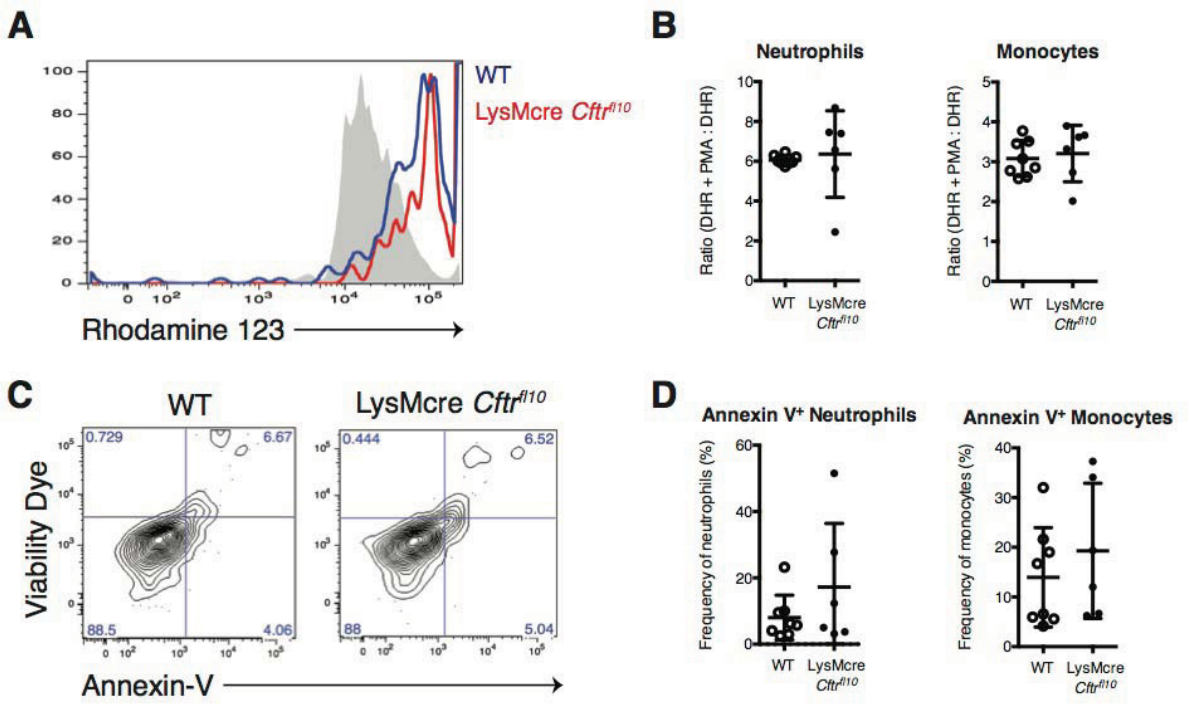

Figure 18. Myeloid cells from myeloid-specific *Cftr*$^{-/-}$ mice have comparable ROS production and apoptosis to WT cells

(A) Representative histogram of Rhodamine 123 signal following the stimulation of neutrophils from the small intestine lamina propria with PMA. Gated on single cells, live cells, CD45^{+}, CD11b^{+}, Ly6G^{+}. **(B)** Oxidative burst activity of steady state CD11b^{+} Ly6G^{+} neutrophils and CD11b^{+} Ly6C^{hi} monocytes from the small intestine of LysMcre CFTR^{fl10} and WT mice (WT n = 8, LysMcre CFTR^{fl10} n = 6). **(C)** Representative contour plot indicating Annexin-V^{+} neutrophils from the small intestine lamina propria. Gated on single cells, live cells, CD45^{+}, CD11b^{+}, Ly6G^{+}. **(D)** Annexin-V staining of CD11b^{+} Ly6G^{+} neutrophils and CD11b^{+} Ly6C^{hi} monocytes from the small intestine of LysMcre CFTR^{fl10} and WT mice at steady state (WT n = 8, LysMcre CFTR^{fl10} n = 6). Values displayed as mean with standard deviation (SD).

4.8 Gut-corrected CF mice are susceptible to *C. rodentium* infection

To address whether the presence of CFTR in the intestinal epithelium provides protection against infection, we infected gut-corrected CF mice with *C. rodentium* and assessed survival. Gut-corrected CF mice harbor a human WT *CFTR* transgene (h*CFTR*) driven by an intestinal promoter (FABP2), allowing for correction of the intestinal phenotype. Upon infection with *C. rodentium*, gut-corrected CF mice were susceptible to infection, with a similar kinetic and mortality rate as ΔF508 mice (Figure 19A). Furthermore, there was significantly higher bacterial burden in the feces of gut-corrected CF mice both at 3DPI and 7DPI compared to WT mice (Figures 19B; 19C). However, FABP2 expression is known to decrease distally along the GI tract, so we decided to assess the degree of CFTR correction in these mice. Upon stimulation with forskolin, an activator specific for CFTR [144], change in current was used as a measure of CFTR function. The ileum of gut-corrected CF mice produced values intermediate to ΔF508 and WT mice, highlighting partial CFTR correction in this tissue (Figure 19D). However, the change in current in the cecum, proximal colon, and distal colon of the gut-corrected CF mice was comparable to ΔF508 levels, indicating a lack of functional CFTR correction in these tissues.

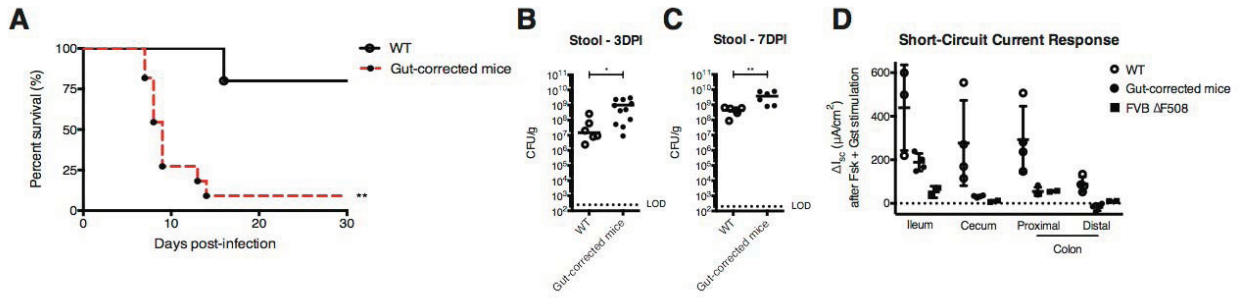

Figure 19. Gut-corrected CF mice are susceptible to C. rodentium infection.
(A) Percent survival of gut-corrected CF (*n* = 11) and WT (*n* = 5) mice following oral infection with *C. rodentium*. **(B)** Bacterial burden in the feces of gut-corrected CF (*n* = 11) and WT (*n* = 6) mice at 3DPI with *C. rodentium*. Line represents the median value. **(C)** Bacterial burden in the feces of gut-corrected CF (*n* = 6) and WT (*n* = 6) mice at 7DPI with *C. rodentium*. Line represents the median value. **(D)** Short circuit current response of CFTR in gut-corrected CF (*n* = 4), WT (*n* = 4), and FVB ΔF508 (*n* = 2) mice after stimulation with forskolin at steady state. Values displayed as mean with standard deviation (SD).

4.9 Wnt signaling is increased in the intestinal stromal cell compartment of ΔF508 mice

Wnt signaling and active β-catenin are critical mediators of intestinal epithelial cell proliferation and differentiation. The impact of CFTR mutation on intestinal homeostasis was addressed via assessment of active β-catenin within the gut lamina propria. ΔF508 mice had significantly higher β-catenin signal within the $CD45^-$ $EpCAM^-$ stromal cell compartment of the small intestine lamina propria when compared to WT mice at steady state (Figure 20B). No differences were observed in β-catenin signal between ΔF508 and WT mice in either the colon or the $CD45^+$ compartment (Figure 20B).

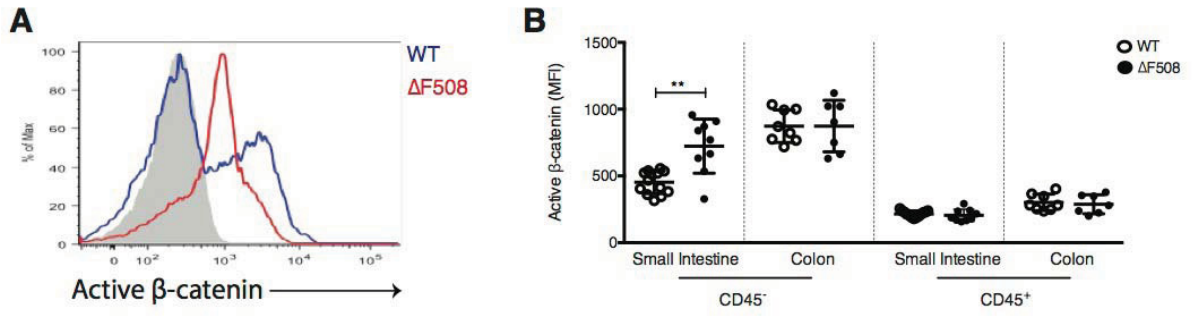

Figure 20. Wnt signaling is increased in the intestinal stromal cell compartment of ΔF508 mice.
(A) Representative histogram of active β-catenin signal within the small intestine lamina propria of ΔF508 and WT mice. Gated on single cells, live cells, $CD45^-$. (B) Median fluorescent intensity (MFI) of active β-catenin within the $CD45^-$ and $CD45^+$ cell compartments of the colon (WT $n = 8$, ΔF508 $n = 7$) and small intestine (WT $n = 13$, ΔF508 $n = 9$) lamina propria of ΔF508 and WT mice at steady state. Values displayed as mean with standard deviation (SD).

Chapter 5: Discussion

Previous investigation into the mechanism of CFTR function in host response to bacterial infection has largely focused on the human lung. While most of the complications in CF pathology are concentrated in lung tissue, there is a major gastrointestinal component in human CF with substantial patient morbidity and mortality. Although murine models of CF do not possess many characteristics similar to human respiratory disease, they do share similar features with the intestinal disease and are considered a good model to study CFTR function in the GI tract [109, 110, 111].

Here we show for the first time that FVB ΔF508 and BALB/c *Cftr*$^{-/-}$ mice are significantly more susceptible than their WT littermates to *C. rodentium* infection (Figure 7), a murine model of EPEC/EHEC infection. Unlike their WT counterparts, both mouse models of CF frequently succumb to the infection and suffer fatal diarrhea. Therefore, we hypothesize that the presence of CFTR in the GI tract is an important factor in the host response to enteric infection.

In most inbred mouse strains, the kinetic of *C. rodentium* infection is well documented [124]. Following oral gavage, *C. rodentium* passes through the GI tract and is initially found in the cecal patch, followed by colonization specifically in the distal colon. The infection is normally contained to the distal region, with detectable levels as early as 3DPI and persisting through bacterial clearance. Our data is the first of its kind showing colonization of *C. rodentium* in tissues other than the distal colon during peak infection.

We have shown an altered localization of *C. rodentium* in ΔF508 mice, with bacteria present in the jejunum, cecum, and proximal colon during infection, with a peak of colonization in the proximal colon (Figure 9). Unlike in ΔF508 mice, *C. rodentium* levels are the highest in the distal colon of WT mice, with fewer bacteria present in proximal tissues. It is interesting to note that CFTR activity is higher in the proximal colon compared to the distal, thus correlating the effects of CFTR on intestinal infection with its expression pattern in the GI tract.

ΔF508 mice have a characteristic mucoviscidosis that leads to intestinal blockage unless mice are kept on a mild laxative. Through immunohistochemistry, the bacteria/mucus interface in the proximal colon of ΔF508 mice was visualized (Figure 8). Importantly, we show that *C. rodentium* associates tightly with the epithelium, allowing for attaching and effacing lesion formation and resulting pathology. Although there is undoubtedly more mucus present in the ΔF508 mice, and a corresponding increase in luminal bacteria, it is unlikely that it is the characteristic mucoviscidosis of ΔF508 mice leading to the observed shift in *C. rodentium* localization.

Infection with an attenuated strain of *C. rodentium* (Δ*espF*) allowed for the analysis of our phenotype over a longer period of time (Figure 10E). At 13DPI, there was a prominent hyperplastic thickening of the proximal colon of ΔF508 mice, which was not present in the distal colon or in WT mice. Thus it appears that the infection in ΔF508 mice persists primarily in the proximal colon, as well as the cecum and regions of the small intestine, and does not undergo delayed migration to the distal colon. These findings may have important implications for the mechanisms of tissue tropism of *C. rodentium*.

Gut-corrected CF mice have a human WT *CFTR* transgene expressed from an intestinal-specific promoter [112]. Although we (Figure 19D) and others [112] have shown that these mice have only partial correction of CFTR function, restricted exclusively to the small intestine, there is no lethal accumulation of mucus and they do not need to be maintained on laxative to survive. However, these mice remain highly susceptible to *C. rodentium* infection (Figure 19A), similar to ΔF508 mice, suggesting that our phenotype is not simply a result of increased intestinal mucus and luminal obstruction. Assessment of bacterial localization and colonization pattern in gut-corrected CF mice would provide further insight into the role of mucus in our model.

Corresponding to an increase in bacterial burden, we observed a greater tissue response to *C. rodentium* infection in the ΔF508 mice, including tissue hyperplasia and increased histopathological measures of disease (Figure 10). Also, we observed significantly higher expression levels of several inflammatory mediators in the proximal colon of ΔF508 mice, including IL-1β, KC, REGIIIβ and REGIII3γ (Figure 11A). IL-1β, secreted primarily by activated macrophages, is an important mediator of the inflammatory response with several implications on innate immune cell function [145]. KC (CXCL1), the murine equivalent of IL-8, is secreted by epithelial cells, macrophages, and neutrophils, and functions primarily as a neutrophil chemoattractant [146]. Lastly, REGIIIβ and REGIIIγ are part of a group of small secretory proteins associated with anti-microbial properties [147]. Together, the increased gene expression of these proteins can be taken as a general readout of inflammation, attributable to the observed differences in bacterial burden and an attempted host response against infection.

In assessing the immune response to infection, there were two major myeloid cell types upregulated at 4DPI with *C. rodentium* in the gut lamina propria of ΔF508 mice compared to WT (Figure 11). Neutrophils and monocytes, as part of the myeloid cell compartment, comprise a major facet of innate immunity to infection. In particular, these cell types are critical in host protection against *C. rodentium* through their phagocytic properties and ROS production. Similar to their immune phenotype during infection, we have shown that ΔF508 mice have significantly higher levels of neutrophils and monocytes in the small intestine at steady state (Figure 13). Considering IL-17 is known to be involved in neutrophil recruitment [148], we hypothesized that it was likely an exaggerated Th17 response leading to the increased neutrophil recruitment in ΔF508 mice. Indeed, we found that there were significantly higher IL-17 producing Th17 cells in the small intestine and colon of ΔF508 mice at steady state (Figure 13). This steady state neutrophil and Th17 driven inflammation is similar to previous observations in the human CF airway [23, 51], and further suggests that our research is a good model to study the CF immune response at mucosal surfaces.

Despite the elevated number of myeloid cell types both at steady state and during infection, ΔF508 mice remain highly susceptible. Ultimately, it appears that the immune system is unable to control the bacteria and falls short in host protection. To evaluate the functional status of myeloid cell types in our model, particularly neutrophils and monocytes, we addressed ROS production and apoptosis rates. At steady state, both neutrophils and monocytes from the small intestine lamina propria of ΔF508 mice produced significantly less ROS compared to WT cells (Figure 14). These ΔF508 cells also had decreased apoptosis compared to WT (Figure 15). There was also a trend towards decreased ICAM-1 (CD54) expression, a leukocyte activation marker,

on ΔF508 neutrophils and monocytes of the small intestine at steady state (Figure 14). In some contexts, increased ICAM-1 expression has been correlated with enhanced ROS production and phagocytosis [143]. It would appear that in our model, decreased ICAM-1 expression supports the data demonstrating depressed function of the ΔF508 myeloid compartment. Not only are these ΔF508 myeloid cells more defective than WT cells, but they also have decreased apoptosis and are not cleared as efficiently, persisting in the lamina propria.

Neutrophil and monocyte effector functions other than ROS production have not been investigated in our model. Evaluation of myeloid phagocytosis in the small intestine lamina propria of ΔF508 mice could be achieved using Zymosan-Texas-Red (ZymTR) *ex vivo* and would further complement our data [143]. We cannot rule out that the sustained quantity of myeloid cell types may be causing off-target effects and resulting tissue pathology in the ΔF508 mice. Investigation into regulatory T cell function and number would provide insight into the relative balance between an effective vs. prolonged destructive immune response in our infection model.

Considering these differences in the ΔF508 myeloid compartment, we initially hypothesized that it was loss of *Cftr* specifically in these cell types leading to the observed phenotype. LysMcre $Cftr^{fl10}$ mice have been shown to be more susceptible to *P. aeruginosa* infection in the lung, compared to WT mice, highlighting an important role of CFTR in myeloid immune cells [42]. In our model, it was surprising that LysMcre $Cftr^{fl10}$ mice were completely resistant to *C. rodentium* infection, similar to WT littermate mice (Figure 17). Furthermore, no defects in ROS production

or apoptosis were observed in the neutrophils or monocytes in the small intestine of these mice at steady state (Figure 18).

It is important to note that genetic background is a major determinant of susceptibility to *C. rodentium* infection [124]. Normally, WT C57BL/6 mice are resistant to infection, with self-limiting colitis of the distal colon [124]. Considering our LysMcre $Cftr^{fl10}$ mice are primarily on a C57BL/6 genetic background, this could potentially be contributing to the observed resistance to infection. However, if loss of CFTR in the myeloid compartment had an important effect on the host response to infection, we would expect to see at least subtle changes in body weight and fecal CFU over the course of infection, which we do not. To further address the role of genetic background in our infection model, we could purchase $Cftr^{-/-}$ mice on a C57BL/6 background and compare infection susceptibility with WT controls.

Another potential explanation for the observed resistance of LysMcre $Cftr^{fl10}$ mice could be inefficient excision of *Cftr* from the myeloid compartment. Although we have shown excision of exon 10 DNA from myeloid cells (Figure 17B), functional CFTR protein could still be reaching the cell membrane. However, this outcome is unlikely considering the importance of exon 10 in protein function. Exon 10 was chosen in the generation of $Cftr^{fl10}$ mice because it is the region of *Cftr* that is commonly mutated in both humans and murine models of CF, particularly ΔF508 [110]. As such, we would expect less than 1% of CFTR protein in the myeloid compartment of our LysMcre $Cftr^{fl10}$ mice [21]. Regardless, absence of CFTR at the protein level should be confirmed in our model through cell sorting and Western blot. Taken together, our results

indicate that loss of CFTR in the myeloid compartment does not compromise the host response to intestinal infection.

To elucidate the relative contribution of CFTR in hematopoietic cells versus resident stromal cells, bone marrow chimera experiments would be beneficial. However, these studies were hindered because ΔF508 mice are on an FVB background and mice with the congenic marker to allow following degree of chimerism are not readily available on this background. As an alternative approach, we decided to investigate myeloid cell function in the bone marrow of ΔF508 mice to determine whether the previously observed myeloid cell defects of the gut lamina propria were related to the tissue environment. When looking in the bone marrow, we found that ΔF508 neutrophils produced significantly less ROS, similar to in the small intestine, although no significant differences were observed between ΔF508 and WT monocytes (Figure 16). Interestingly, no differences in apoptosis were observed for either cell type in the bone marrow (Figure 16). This phenotype is also observed with the neutrophils of CF patients. Although CF neutrophils have decreased apoptosis in the lung [38], deficiencies in apoptosis have not been observed in the peripheral blood [149], suggesting that it is the interaction with airway epithelial cells leading to myeloid cell apoptosis. In our model, it is conceivable that the observed myeloid cell defects are a consequence of interaction with the intestinal epithelium of ΔF508 mice.

We are unable to draw conclusions when assessing the susceptibility of our gut-corrected CF mice to infection with *C. rodentium*. We noted partial CFTR correction restricted to the small intestine, making it difficult to determine the relative contribution of CFTR in the intestinal epithelium in host protection against infection. Therefore, we are currently breeding Vil1-cre

mice with *Cftr*^{fl10} mice, allowing for *Cftr* inactivation in villus and crypt epithelial cells of the intestine. Susceptibility to infection in these mice would support the hypothesis that functional CFTR mediates host protection in an intestinal epithelial cell dependent manner. Interestingly, the localization pattern of *C. rodentium* in ΔF508 mice corresponds well with the expression pattern of CFTR in the murine gut [71]. This data further suggests that under WT conditions, CFTR functions to protect the GI tract from intestinal infection in regions proximal to the distal colon.

It remains to be addressed how loss of CFTR function in the intestinal epithelium might lead to our observed phenotype. It has been well documented that microbial dysbiosis can influence gut homeostasis, with several species capable of shifting the host immune system. In particular, segmented filamentous bacteria have been shown to cause a Th17 cell bias, through activation of the intestinal epithelium [150]. Additionally, is not uncommon for CF mice, and patients, to have dysbiosis of the gut microbiota. Lactobacillus, bifidobacterium, and *Escherichia coli* have been found in excess in the gut of either murine or human CF populations [87, 151, 152]. Furthermore, it has been shown that the depletion of these species can influence some of the steady state inflammation observed in the CF gut [153]. Although our *Cftr* mutant mice are co-housed with WT littermates, we cannot rule out the possibility that CFTR dysfunction is attributing to the persistent immune phenotype in ΔF508 mice through microbial dysbiosis. Microbiome screening through 16S rRNA sequencing would provide us with a more complete picture of our model. Furthermore, selective bacterial depletion with antibiotics may provide insight into the role of some of the major communities within the ΔF508 microbiome.

Another possible contributor to our phenotype is the effect of CFTR on Wnt signaling in the gut. Recently, it has been shown that *Cftr* functions as a tumor suppressor gene through alteration of Wnt β-catenin target genes [105]. Also, our lab has shown that increased Wnt signaling can drive loss of differentiation of the intestinal epithelium and directly cause mortality during *C. rodentium* infection through loss of intestinal function [138]. In our model, we have shown that ΔF508 mice have increased active β-catenin compared to WT mice in the stromal cell compartment of the small intestine lamina propria (Figure 20). This is likely resulting in a hyper proliferative and dedifferentiated intestinal epithelium, negatively affecting intestinal function. The expression level of various Wnt target genes in ΔF508 mice, such as *Axin2*, *Mmp7*, and *Myc*, should be investigated further both at steady state and during infection. Furthermore, staining for these markers by immunohistochemistry and proliferating cell nuclear antigen (PCNA) staining for proliferation would help to delineate differences in intestinal homeostasis as a result of CFTR dysfunction. Lastly, the upstream signals leading to β-catenin accumulation remain to be elucidated.

Whether CF patients have an increased incidence of intestinal infection has yet to be determined. However, children with CF have been shown to have an *E. coli* dysbiosis of their gut microbiota, correlating with poorer GI function [152]. Whatever is driving this dysbiosis in the CF gut is likely the causative agent of our *C. rodentium* phenotype. Therefore, we believe that *C. rodentium* infection provides a model to study intestinal disease observed in CF patients. Furthermore, as the life expectancy of CF patients continues to grow and intestinal morbidity becomes more prevalent, our research provides a complementary model to study the role of CFTR at mucosal surfaces and CFTR biology as a whole.

References

1. Cutting GR. Modifier genetics: cystic fibrosis. Annu Rev Genomics Hum Genet 2005;6:237–60.
2. Stephenson AL, Tom M, Berthiaume Y, et al. A contemporary survival analysis of individuals with cystic fibrosis: a cohort study. Eur Respir J. 2015 Mar;45(3):670-9.
3. Riordan JR, Rommens JM, Kerem B, et al. Identification of the cystic fibrosis gene: cloning and characterization of complementary DNA. Science 1989;245:1066–73.
4. McCarty NA. Permeation through the CFTR chloride channel. J Exp Biol 2000;203:1947–62.
5. Vankeerberghen A, Cuppens H, Cassiman JJ. The cystic fibrosis transmembrane conductance regulator: an intriguing protein with pleiotropic functions. J Cyst Fibros 2002;1:13–29
6. Gregory RJ, Cheng SH, Rich DP, et al. Expression and characterization of the cystic fibrosis transmembrane conductance regulator. Nature 1990;347:382–6.
7. Frizzell RA. Ten years with CFTR. Physiol Rev 1999;79:S1–2.
8. Kerem B, Rommens JM, Buchanan WJ, et al.: Identification of the cystic fibrosis gene: genetic analysis. Science 1989, 245:1073–1080.
9. Higgins C. ABC transporters: from microorganisms to man. Annu Rev Cell Biol 1992;8:67–113.
10. Gadsby DC, Vergani P, Csanády L. The ABC protein turned chloride channel whose failure causes cystic fibrosis. Nature 2006;440:477–83.
11. Rosenberg MF, O'Ryan LP, Hughes G, et al. The cystic fibrosis transmembrane conductance regulator (CFTR): three-dimensional structure and localization of a channel gate. J Biol Chem 2011;286:42647–54.
12. Riordan JR. CFTR function and prospects for therapy. Annu Rev Biochem 2008;77:701–26.
13. Higgins CF, Linton KJ. The ATP switch model for ABC transporters. Nat Struct Mol Biol 2004;11:918–26.
14. Chappe V, Irvine T, Liao J, et al. Phosphorylation of CFTR by PKA promotes binding of the regulatory domain. EMBO J 2005; 24(15):2730–2740.

15. Cheng SH, Rich DP, Marshall J, et al. Phosphorylation of the R domain by cAMP-dependent protein kinase regulates the CFTR chloride channel. Cell 1991;66:1027–36.
16. Frizzell RA, Hanrahan JW. Physiology of epithelial chloride and fluid secretion. Cold Spring Harb Perspect Med. 2012 Jun;2(6):a009563.
17. Ferec C, Cutting GR. Assessing the Disease-Liability of Mutations in CFTR. Cold Spring Harb Perspect Med. 2012 Dec 1;2(12):a009480.
18. Hwang TC, Wang F, Yang IC, et al. Genistein potentiates wild-type and deltaF508-CFTR channel activity. Am J Physiol 1997;273:C988–98.
19. Kazazian HH Jr. Population variation of common cystic fibrosis mutations: the cystic fibrosis genetic analysis consortium. Hum Mutat 1994, 4:167–177.
20. O'Sullivan BP, Freedman SD. Cystic fibrosis. Lancet. 2009 May 30;373(9678):1891-904.
21. Lukacs GL, Verkman AS. CFTR: folding, misfolding and correcting the ΔF508 conformational defect. Trends in molecular medicine. 2012;18(2):81-91. doi:10.1016/j.molmed.2011.10.003.
22. Zielenski J1. Genotype and phenotype in cystic fibrosis. Respiration. 2000;67(2):117-33.
23. Cohen TS, Prince A. Cystic fibrosis: a mucosal immunodeficiency syndrome. Nat Med. 2012 Apr 5;18(4):509-19.
24. Mogensen TH. Pathogen Recognition and Inflammatory Signaling in Innate Immune Defenses. Clinical Microbiology Reviews. 2009;22(2):240-273.
25. Vij N, Mazur S, Zeitlin PL. CFTR is a negative regulator of NFkappaB mediated innate immune response. PLoS One. 2009;4(2):e4664.
26. Bérubé J, Roussel L, Nattagh L, et al. Loss of cystic fibrosis transmembrane conductance regulator function enhances activation of p38 and ERK MAPKs, increasing interleukin-6 synthesis in airway epithelial cells exposed to Pseudomonas aeruginosa. J Biol Chem. 2010 Jul 16;285(29):22299-307.
27. Greene CM, Carroll TP, Smith SG, et al. TLR-induced inflammation in cystic fibrosis and non-cystic fibrosis airway epithelial cells. J Immunol. 2005 Feb 1;174(3):1638-46.
28. Kunkel SL, Standiford T, Kasahara K, et al. Interleukin-8 (IL-8): the major neutrophil chemotactic factor in the lung. Exp Lung Res. 1991 Jan-Feb;17(1):17-23.
29. Saba S, Soong G, Greenberg S, et al. Bacterial stimulation of epithelial G-CSF and GM-CSF expression promotes PMN survival in CF airways. Am J Respir Cell Mol Biol. 2002

Nov;27(5):561-7.

30. Kruger P, Saffarzadeh M, Weber ANR, et al. Neutrophils: Between Host Defence, Immune Modulation, and Tissue Injury. Dehio C, ed. PLoS Pathogens. 2015;11(3):e1004651.
31. Gao L, Kim KJ, Yankaskas JR, et al. Abnormal glutathione transport in cystic fibrosis airway epithelia. Am J Physiol. 1999 Jul;277(1 Pt 1):L113-8.
32. Xu Y, Szép S, Lu Z. The antioxidant role of thiocyanate in the pathogenesis of cystic fibrosis and other inflammation-related diseases. Proc Natl Acad Sci U S A. 2009 Dec 1;106(48):20515-9.
33. Hudson VM. Rethinking cystic fibrosis pathology: the critical role of abnormal reduced glutathione (GSH) transport caused by CFTR mutation. Free Radic Biol Med. 2001 Jun 15;30(12):1440-61.
34. Bartling TR, Drumm ML. Oxidative stress causes IL8 promoter hyperacetylation in cystic fibrosis airway cell models. Am J Respir Cell Mol Biol. 2009 Jan;40(1):58-65.
35. Ulrich M, Worlitzsch D, Viglio S, et al. Alveolar inflammation in cystic fibrosis. J Cyst Fibros. 2010 May;9(3):217-27.
36. Matsui H, Verghese MW, Kesimer M, et al. Reduced three-dimensional motility in dehydrated airway mucus prevents neutrophil capture and killing bacteria on airway epithelial surfaces. J Immunol. 2005 Jul 15;175(2):1090-9.
37. Alexis NE, Muhlebach MS, Peden DB, et al. Attenuation of host defense function of lung phagocytes in young cystic fibrosis patients. J Cyst Fibros. 2006 Jan;5(1):17-25.
38. Downey DG, Brockbank S, Martin SL, et al. The effect of treatment of cystic fibrosis pulmonary exacerbations on airways and systemic inflammation. Pediatr Pulmonol. 2007 Aug;42(8):729-35.
39. Ratner D, Mueller C. Immune responses in cystic fibrosis: are they intrinsically defective? Am J Respir Cell Mol Biol. 2012 Jun;46(6):715-22.
40. Hayes E, Pohl K, McElvaney NG, et al. The cystic fibrosis neutrophil: a specialized yet potentially defective cell. Arch Immunol Ther Exp (Warsz). 2011 Apr;59(2):97-112.
41. Adib-Conquy M, Pedron T, Petit-Bertron A-F, et al. Neutrophils in Cystic Fibrosis Display a Distinct Gene Expression Pattern. Molecular Medicine. 2008;14(1-2):36-44.
42. Bonfield TL, Hodges CA, Cotton CU, et al. Absence of the cystic fibrosis transmembrane

regulator (Cftr) from myeloid-derived cells slows resolution of inflammation and infection. Journal of Leukocyte Biology. 2012;92(5):1111-1122.

43. Painter RG, Valentine VG, Lanson NA, et al. CFTR Expression in Human Neutrophils and the Phagolysosomal Chlorination Defect in Cystic Fibrosis. Biochemistry. 2006;45(34):10260-10269.
44. Hartl D, Griese M, Kappler M, et al. Pulmonary T(H)2 response in Pseudomonas aeruginosa-infected patients with cystic fibrosis. J Allergy Clin Immunol. 2006 Jan;117(1):204-11.
45. McAllister F1, Henry A, Kreindler JL, et al. Role of IL-17A, IL-17F, and the IL-17 receptor in regulating growth-related oncogene-alpha and granulocyte colony-stimulating factor in bronchial epithelium: implications for airway inflammation in cystic fibrosis. J Immunol. 2005 Jul 1;175(1):404-12.
46. Decraene A, Willems-Widyastuti A, Kasran A, et al. Elevated expression of both mRNA and protein levels of IL-17A in sputum of stable Cystic Fibrosis patients. Respir Res. 2010 Dec 10;11:177.
47. Sokol CL, Chu NQ, Yu S, et al. Basophils function as antigen-presenting cells for an allergen-induced T helper type 2 response. Nat Immunol. 2009 Jul;10(7):713-20.
48. Luckheeram RV, Zhou R, Verma AD, et al. CD4$^+$T cells: differentiation and functions. Clin Dev Immunol. 2012;2012:925135.
49. Mueller C, Braag SA, Keeler A, et al. Lack of cystic fibrosis transmembrane conductance regulator in CD3+ lymphocytes leads to aberrant cytokine secretion and hyperinflammatory adaptive immune responses. Am J Respir Cell Mol Biol. 2011 Jun;44(6):922-9.
50. Huber S, Gagliani N, Flavell RA. Life, death, and miracles: Th17 cells in the intestine. Eur J Immunol. 2012 Sep;42(9):2238-45.
51. Tan H-L, Regamey N, Brown S, et al. The Th17 Pathway in Cystic Fibrosis Lung Disease. American journal of respiratory and critical care medicine. 2011;184(2):252-258.
52. Miossec P, Kolls JK. Targeting IL-17 and TH17 cells in chronic inflammation. Nat Rev Drug Discov. 2012 Oct;11(10):763-76.
53. Kushwah R, Gagnon S, Sweezey NB1. Intrinsic predisposition of naïve cystic fibrosis T

cells to differentiate towards a Th17 phenotype. Respir Res. 2013 Dec 17;14:138.

54. Waite JC, Skokos D. Th17 response and inflammatory autoimmune diseases. Int J Inflam. 2012 ;2012:819467.
55. Artis D. Epithelial-cell recognition of commensal bacteria and maintenance of immune homeostasis in the gut. Nat Rev Immunol. 2008 Jun;8(6):411-20.
56. Peterson LW, Artis D. Intestinal epithelial cells: regulators of barrier function and immune homeostasis. Nat Rev Immunol. 2014 Mar;14(3):141-53.
57. Round JL, Mazmanian SK. The gut microbiome shapes intestinal immune responses during health and disease. Nature reviews Immunology. 2009 ;9(5):313-323.
58. Crosnier C, Stamataki D, Lewis J. Organizing cell renewal in the intestine: stem cells, signals and combinatorial control. Nature Rev. Genet. 2006 7, 349–359.
59. Van der Flier LG, Clevers H. Stem cells, self-renewal, and differentiation in the intestinal epithelium. Annu. Rev. Physiol. 2009;71, 241–260.
60. Kim YS, Ho SB. Intestinal goblet cells and mucins in health and disease: recent insights and progress. Curr. Gastroenterol. Rep. 2010;12, 319–330.
61. Johansson MEV, et al. The inner of the two Muc2 mucin-dependent mucus layers in colon is devoid of bacteria. Proc. Natl Acad. Sci. 2008;105, 15064–15069.
62. Gallo RL, Hooper LV. Epithelial antimicrobial defence of the skin and intestine. Nature Rev. Immunol. 2012;12, 503–516.
63. Bevins CL, Salzman NH. Paneth cells, antimicrobial peptides and maintenance of intestinal homeostasis. Nature Rev. Microbiol. 2011;9, 356–368.
64. Abreu MT. Toll-like receptor signalling in the intestinal epithelium: how bacterial recognition shapes intestinal function. Nature Rev. Immunol. 2010;10, 131–144.
65. Chen GY, Núñez G. Inflammasomes in intestinal inflammation and cancer. Gastroenterology 2011;141, 1986–1999.
66. Elinav E, Henao-Mejia J, Flavell RA. Integrative inflammasome activity in the regulation of intestinal mucosal immune responses. Mucosal Immunol. 2013;6, 4–13.
67. Li XD, et al. Mitochondrial antiviral signaling protein (MAVS) monitors commensal bacteria and induces an immune response that prevents experimental colitis. Proc. Natl Acad. Sci. 2011;108, 17390–17395.
68. Broquet AH, Hirata Y, McAllister CS, et al. RIG-I/MDA5/MAVS are required to signal a

protective IFN response in rotavirus-infected intestinal epithelium. J. Immunol. 2011;186, 1618–1626.

69. Mabbott NA, Donaldson DS, Ohno H, et al. Microfold (M) cells: important immunosurveillance posts in the intestinal epithelium. Mucosal Immunol. 2013;6, 666–677.
70. Wilschanski M, Durie PR. Patterns of GI disease in adulthood associated with mutations in the CFTR gene. Gut. 2007;56(8):1153-1163. doi:10.1136/gut.2004.062786.
71. Strong TV, Boehm K, Collins FS. Localization of cystic fibrosis transmembrane conductance regulator mRNA in the human gastrointestinal tract by in situ hybridization. J Clin Invest. 1994 Jan;93(1):347-54.
72. Kreda SM, Davis CW, Rose MC. CFTR, Mucins, and Mucus Obstruction in Cystic Fibrosis. Cold Spring Harbor Perspectives in Medicine. 2012;2(9):a009589. doi:10.1101/cshperspect.a009589.
73. De Lisle RC, Borowitz D. The cystic fibrosis intestine. Cold Spring Harb Perspect Med. 2013 Sep 1;3(9):a009753.
74. Crawford I1, Maloney PC, Zeitlin PL, et al. Immunocytochemical localization of the cystic fibrosis gene product CFTR. Proc Natl Acad Sci U S A. 1991 Oct 15;88(20):9262-6.
75. Briel M, Greger R, Kunzelmann K. Cl-transport by cystic fibrosis transmembrane conductance regulator (CFTR) contributes to the inhibition of epithelial Na+ channels (ENaCs) in Xenopus oocytes co-expressing CFTR and ENaC. J Physiol 1998;508(Pt 3):825–36.
76. Boucher RC. Cystic fibrosis: a disease of vulnerability to airway surface dehydration. Trends Mol Med 2007;13:231–40.
77. Feingold J, Guilloud-Bataille M. Genetic comparisons of patients with cystic fibrosis with or without meconium ileus. Clinical Centers of the French CF Registry. Adv Genet 1999;42:147–50.
78. Cleghorn GJ, Stringer DA, Forstner GG, et al. Treatment of distal intestinal obstruction syndrome in cystic fibrosis with a balanced intestinal lavage solution. Lancet. 1986 Jan 4; 1(8471):8-11.
79. Houwen RH, van der Doef HP, Sermet I, et al. Defining DIOS and constipation in cystic

fibrosis with a multicentre study on the incidence, characteristics, and treatment of DIOS. J Pediatr Gastroenterol Nutr. 2010 Jan;50(1):38-42.

80. Dray X, Bienvenu T, Desmazes-Dufeu N, et al. Distal intestinal obstruction syndrome in adults with cystic fibrosis. Clin Gastroenterol Hepatol, 2 (2004), pp. 498–503.
81. De Lisle RC, Roach EA, Norkina O. Eradication of small intestinal bacterial overgrowth in the cystic fibrosis mouse reduces mucus accumulation. J Pediatr Gastroenterol Nutr 2006;42: 46–52.
82. Malmberg EK, Noaksson KA, Phillipson M, et al. Increased levels of mucins in the cystic fibrosis mouse small intestine and modulator effects of the Muc1 mucin expression. Am J Physiol Gastrointest Liver Physiol 2006;291: G203–G210.
83. De Lisle RC, Roach E, Jansson K. Effects of laxative and N-acetylcysteine on mucus accumulation, bacterial load, transit, and inflammation in the cystic fibrosis mouse small intestine. Am J Physiol Gastrointest Liver Physiol. 2007 Sep;293(3):G577-84.
84. Lewindon PJ, Robb TA, Moore DJ, et al. Bowel dysfunction in cystic fibrosis: importance of breath testing. J Paediatr Child Health. 1998 Feb;34(1):79-82.
85. Norkina O, Burnett TG, De Lisle RC. Bacterial Overgrowth in the Cystic Fibrosis Transmembrane Conductance Regulator Null Mouse Small Intestine . Infection and Immunity. 2004;72(10):6040-6049.
86. De Lisle RC. Altered transit and bacterial overgrowth in the cystic fibrosis mouse small intestine. Am J Physiol Gastrointest Liver Physiol. 2007 Jul;293(1):G104-11.
87. Lynch SV, Goldfarb KC, Wild YK, et al. Cystic fibrosis transmembrane conductance regulator knockout mice exhibit aberrant gastrointestinal microbiota. Gut Microbes. 2013 Jan-Feb;4(1):41-7.
88. Durmaz B, Dalgalar M, Durmaz R. Prevalence of enterotoxigenic Bacteroides fragilis in patients with diarrhea: a controlled study. Anaerobe. 2005 Dec;11(6):318-21.
89. Clarke LL, Gawenis LR, Bradford EM, et al. Abnormal Paneth cell granule dissolution and compromised resistance to bacterial colonization in the intestine of CF mice. Am J Physiol Gastrointest Liver Physiol. 2004 Jun;286(6):G1050-8.
90. Bazett M, Honeyman L, Stefanov AN, et al. Cystic fibrosis mouse model-dependent intestinal structure and gut microbiome. Mamm Genome. 2015 Jun;26(5-6):222-34.
91. Duytschaever G, Huys G, Bekaert M, et al. Cross-sectional and longitudinal comparisons

of the predominant fecal microbiota compositions of a group of pediatric patients with cystic fibrosis and their healthy siblings. Appl Environ Microbiol. 2011 Nov;77(22):8015-24.

92. Duytschaever G, Huys G, Bekaert M, et al. Dysbiosis of bifidobacteria and Clostridium cluster XIVa in the cystic fibrosis fecal microbiota. J Cyst Fibros. 2013 May;12(3):206-15.
93. Hoffman LR, Pope CE, Hayden HS, et al. Escherichia coli dysbiosis correlates with gastrointestinal dysfunction in children with cystic fibrosis. Clin Infect Dis. 2014 Feb;58(3):396-9.
94. Madan JC, Koestler DC, Stanton BA, et al. Serial Analysis of the Gut and Respiratory Microbiome in Cystic Fibrosis in Infancy: Interaction between Intestinal and Respiratory Tracts and Impact of Nutritional Exposures. mBio. 2012;3(4):e00251-12.
95. Norkina O, Kaur S, Ziemer D, et al. Inflammation of the cystic fibrosis mouse small intestine. Am J Physiol Gastrointest Liver Physiol. 2004 Jun;286(6):G1032-41.
96. Knorre A, Wagner M, Schaefer HE, et al. DeltaF508-CFTR causes constitutive NF-kappaB activation through an ER-overload response in cystic fibrosis lungs. Biol Chem. 2002 Feb;383(2):271-82.
97. Weber AJ, Soong G, Bryan R, et al. Activation of NF-kappaB in airway epithelial cells is dependent on CFTR trafficking and Cl- channel function. Am J Physiol Lung Cell Mol Physiol. 2001 Jul;281(1):L71-8.
98. O'Donnell LC, Druhan LJ, Avalos BR. Molecular characterization and expression analysis of leucine-rich alpha2-glycoprotein, a novel marker of granulocytic differentiation. J Leukoc Biol. 2002 Sep;72(3):478-85.
99. Kruger P, Saffarzadeh M, Weber ANR, et al. Neutrophils: Between Host Defence, Immune Modulation, and Tissue Injury. Dehio C, ed. PLoS Pathogens. 2015;11(3):e1004651.
100. Bruno MJ, Haverkort EB, Tytgat GN, et al. Maldigestion associated with exocrine pancreatic insufficiency: implications of gastrointestinal physiology and properties of enzyme preparations for a cause-related and patient-tailored treatment. Am J Gastroenterol. 1995 Sep;90(9):1383-93.
101. Fieker A, Philpott J, Armand M. Enzyme replacement therapy for pancreatic

insufficiency: present and future. Clinical and Experimental Gastroenterology. 2011;4:55-73.

102. Colombo C, Battezzati PM. Hepatobiliary manifestations of cystic fibrosis. Eur J Gastroenterol Hepatol. 1996 Aug;8(8):748-54.
103. Akata D, Akhan O, Ozcelik U, et al. Hepatobiliary manifestations of cystic fibrosis in children: correlation of CT and US findings. Eur J Radiol. 2002 Jan;41(1):26-33.
104. Audeh MW. Gastrointestinal cancer and the cystic fibrosis gene. N Engl J Med 1995; 333:129-130
105. Than BL, Linnekamp JF, Starr TK, et al. CFTR is a tumor suppressor gene in murine and human intestinal cancer. Oncogene. 2016 Jan 11. [Epub ahead of print]
106. Logan CY, Nusse R. The Wnt signaling pathway in development and disease. Annual review of cell and developmental biology. 2004;20:781–810.
107. MacDonald BT, Tamai K, He X. Wnt/β-catenin signaling: components, mechanisms, and diseases. Developmental cell. 2009;17(1):9-26.
108. Schuijers J, Clevers H. Adult mammalian stem cells: the role of Wnt, Lgr5 and R-spondins. The EMBO Journal. 2012;31(12):2685-2696.
109. Snouwaert JN, Brigman KK, Latour AM, et al. An animal model for cystic fibrosis made by gene targeting. Science 1992;257:1083–8.
110. Hodges CA, Cotton CU, Palmert MR, et al. Generation of a conditional null allele for *Cftr* in mice. Genesis (New York, NY : 2000). 2008;46(10):546-552.
111. Ehre C, Ridley C, Thornton DJ. Cystic fibrosis: an inherited disease affecting mucin-producing organs. Int J Biochem Cell Biol. 2014 Jul;52:136-45.
112. Zhou L, Dey CR, Wert SE, et al. Correction of lethal intestinal defect in a mouse model of cystic fibrosis by human CFTR. Science. 1994 Dec 9;266(5191):1705-8.
113. Wang TY, Liu M, Portincasa P, et al. New insights into the molecular mechanism of intestinal fatty acid absorption. European journal of clinical investigation. 2013;43(11):1203-1223. Nataro, J. P. & Kaper, J. B. Diarrheagenic Escherichia coli. Clin. Microbiol. Rev. 1998;11, 142–201.
114. Nataro JP, Kaper JB. Diarrheagenic Escherichia coli. Clin. Microbiol. Rev. 1998;11, 142–201.
115. Bray J. Isolation of antigenically homogeneous strains of Bact. coli neopolitanum from

summer diarrhoea of infants. J. Pathol. Bacteriol. 1945;57, 239–247.

116. Frankel G, Phillips AD. Attaching effacing Escherichia coli and paradigms of Tir-triggered actin polymerization: getting off the pedestal. Cell. Microbiol. 2008;10, 549–556.
117. Frankel G, et al. Enteropathogenic and enterohaemorrhagic Escherichia coli: more subversive elements. Mol. Microbiol. 1998;30, 911–921.
118. Fagundes-Neto U, Kallas MR, Patricio FR. Morphometric study of the small bowel mucosa in infants with diarrhea due to enteropathogenic Escherichia coli strains. Hepatogastroenterology 1997;44, 1051–1056.
119. Karch H. The role of virulence factors in enterohemorrhagic Escherichia coli (EHEC)–associated hemolytic-uremic syndrome. Semin. Thromb. Hemost. 2001;27, 207–213.
120. Collins JW, Keeney KM, Crepin VF, et al. Citrobacter rodentium: infection, inflammation and the microbiota. Nat Rev Microbiol. 2014 Sep;12(9):612-23.
121. Schauer DB, Falkow S. Attaching and effacing locus of a Citrobacter freundii biotype that causes transmissible murine colonic hyperplasia. Infect. Immun. 1993;61, 2486–2492.
122. Deng W, Vallance BA, Li Y, et al. Citrobacter rodentium translocated intimin receptor (Tir) is an essential virulence factor needed for actin condensation, intestinal colonization and colonic hyperplasia in mice. Mol. Microbiol. 2003;48, 95–115.
123. Petty NK, et al. The Citrobacter rodentium genome sequence reveals convergent evolution with human pathogenic Escherichia coli. J. Bacteriol. 2010;192, 525–538.
124. Mundy R, MacDonald TT, Dougan G, et al. Citrobacter rodentium of mice and man. Cell Microbiol. 2005 Dec;7(12):1697-706.
125. Higgins LM, Frankel G, Douce G, et al. Citrobacter rodentium infection in mice elicits a mucosal T_H1 cytokine response and lesions similar to those in murine inflammatory bowel disease. Infection Immun. 1999;67, 3031–3039.
126. Wiles S, Pickard KM, Peng K, et al. In vivo bioluminescence imaging of the murine pathogen Citrobacter rodentium. Infect. Immun. 2006;74, 5391–5396.
127. Gibson DL, et al. Toll-like receptor 2 plays a critical role in maintaining mucosal integrity during Citrobacter rodentium-induced colitis. Cell. Microbiol. 2008;10, 388–403.

128. Khan MA, et al. Toll-like receptor 4 contributes to colitis development but not to host defense during Citrobacter rodentium infection in mice. Infection Immun. 2006;74, 2522–2536.
129. Lebeis SL, Bommarius B, Parkos CA, et al. TLR signaling mediated by MyD88 is required for a protective innate immune response by neutrophils to Citrobacter rodentium. J. Immunol. 2007;179, 566–577.
130. Gibson D, et al. MyD88 signalling plays a critical role in host defence by controlling pathogen burden and promoting epithelial cell homeostasis during Citrobacter rodentium-induced colitis. Cell. Microbiol. 2008;10, 618–631.
131. Bergstrom KS, Sham HP, Zarepour M, et al. Innate host responses to enteric bacterial pathogens: a balancing act between resistance and tolerance. Cell. Microbiol. 2012;14, 475–484.
132. Kayagaki N, et al. Non-canonical inflammasome activation targets caspase-11. Nature. 2011;479, 117–121.
133. Simmons CP, et al. Central role for B lymphocytes and $CD4^+$ T cells in immunity to infection by the attaching and effacing pathogen Citrobacter rodentium. Infection Immun. 2003;71, 5077–5086.
134. Vallance BA, Deng W, Knodler LA, et al. Mice lacking T and B lymphocytes develop transient colitis and crypt hyperplasia yet suffer impaired bacterial clearance during Citrobacter rodentium infection. Infection Immun. 2002;70, 2070–2081.
135. Mangan PR, et al. Transforming growth factor-β induces development of the T_H17 lineage. Nature. 2006; 441, 231–234.
136. Torchinsky MB, Garaude J, Martin AP, et al. Innate immune recognition of infected apoptotic cells directs T_H17 cell differentiation. Nature. 2009;458, 78–82.
137. Zheng, Y. et al. Interleukin-22 mediates early host defense against attaching and effacing bacterial pathogens. Nature Med. 2008;14, 282–289.
138. Papapietro O, Teatero S, Thanabalasuriar A, et al. R-spondin 2 signalling mediates susceptibility to fatal infectious diarrhoea. Nat Commun. 2013;4:1898.
139. Jin YR, Yoon JK. The R-spondin family of proteins: emerging regulators of WNT signaling. Int J Bio- chem Cell Biol. 2012; 44:2278–2287.
140. Sato T, Vries RG, Snippert HJ, van de Wetering M, et al. Single Lgr5 stem cells build

crypt-villus structures in vitro without a mesenchymal niche. Nature. 2009; 459:262–265

141. Bergstrom KSB, Guttman JA, Rumi M, et al. Modulation of Intestinal Goblet Cell Function during Infection by an Attaching and Effacing Bacterial Pathogen. Infection and Immunity. 2008;76(2):796-811.
142. Weigmann B, Tubbe I, Seidel D, et al. Isolation and subsequent analysis of murine lamina propria mononuclear cells from colonic tissue. Nat Protoc. 2007; 2:2307–2311.
143. Woodfin A, Beyrau M, Voisin MB, et al. ICAM-1-expressing neutrophils exhibit enhanced effector functions in murine models of endotoxemia. Blood. 2016 Feb 18;127(7):898-907.
144. Haws CM, Nepomuceno IB, Krouse ME, et al. Delta F508-CFTR channels: kinetics, activation by forskolin, and potentiation by xanthines. Am J Physiol. 1996 May;270(5 Pt 1):C1544-55.
145. Dinarello CA. Immunological and inflammatory functions of the interleukin-1 family. Annu Rev Immunol. 2009;27:519-50.
146. Kobayashi Y. Neutrophil infiltration and chemokines. Crit Revs Immunol. 2006;26:307–315.
147. Parikh A, Stephan A-F, Tzanakakis ES. Regenerating proteins and their expression, regulation and signaling. Biomolecular concepts. 2012;3(1):57-70.
148. Ouyang W, Kolls JK, Zheng Y. The biological functions of T helper 17 cell effector cytokines in inflammation. Immunity 2008;28(4):454-467.
149. Houston N, Stewart N, Smith DS, Bell SC, et al. Sputum neutrophils in cystic fibrosis patients display a reduced respiratory burst. J Cyst Fibros. 2013 Jul;12(4):352-62.
150. Ivanov II, Atarashi K, Manel N, et al. Induction of intestinal Th17 cells by segmented filamentous bacteria. Cell. 2009;139(3):485-498. doi:10.1016/j.cell.2009.09.033.
151. Duytschaever G1, Huys G, Bekaert M, et al. Dysbiosis of bifidobacteria and Clostridium cluster XIVa in the cystic fibrosis fecal microbiota. J Cyst Fibros. 2013 May;12(3):206-15.
152. Hoffman LR, Pope CE, Hayden HS, et al. *Escherichia coli* dysbiosis correlates with gastrointestinal dysfunction in children with cystic fibrosis. Clin Infect Dis. 2014; 58:396– 399.
153. Bazett M, Bergeron M-E, Haston CK. Streptomycin treatment alters the intestinal

microbiome, pulmonary T cell profile and airway hyperresponsiveness in a cystic fibrosis mouse model. Scientific Reports. 2016;6:19189.

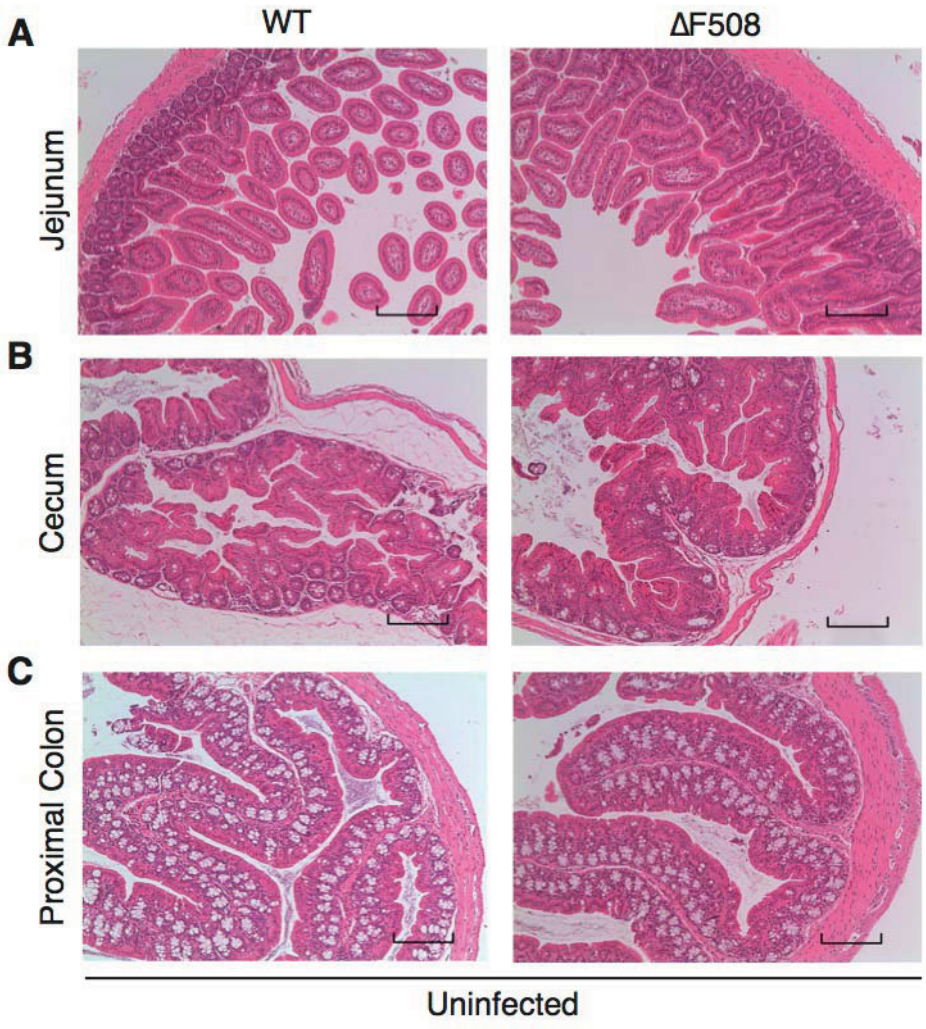

Appendix 1. No overt differences in tissue architecture and architecture between WT and ΔF508 mice at steady state.
H&E stain of **(A)** jejunum, **(B)** cecum and **(C)** proximal colon tissues of uninfected WT and ΔF508 mice (10X magnification). Scale bars are 300 micron.

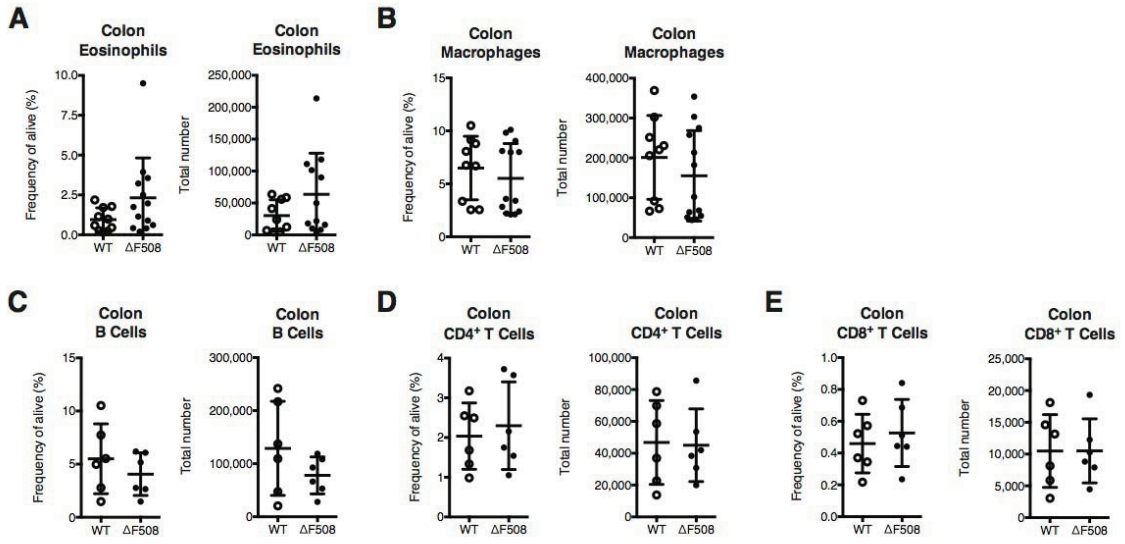

Appendix 2. Immunophenotyping of the colon lamina propria at 4DPI with *C. rodentium*.
Frequency and total number of **(A)** SSC^{hi} Siglec-F^{+} eosinophils in the colon of ΔF508 (*n* = 13) and WT (*n* = 9) mice at 4DPI with *C. rodentium*. **(B)** $CD11b^{+}$ $F4/80^{+}$ macrophages in the colon of ΔF508 (*n* = 13) and WT (*n* = 9) mice at 4DPI with *C. rodentium*. **(C)** $TCR\beta^{-}$ $CD19^{+}$ B cells in the colon of ΔF508 (*n* = 6) and WT (*n* = 6) mice at 4DPI with *C. rodentium*. **(D)** $TCR\beta^{+}$ $CD4^{+}$ T cells in the colon of ΔF508 (*n* = 6) and WT (*n* = 6) mice at 4DPI with *C. rodentium*. **(E)** $TCR\beta^{+}$ $CD8^{+}$ T cells in the colon of ΔF508 (*n* = 6) and WT (*n* = 6) mice at 4DPI with *C. rodentium*.

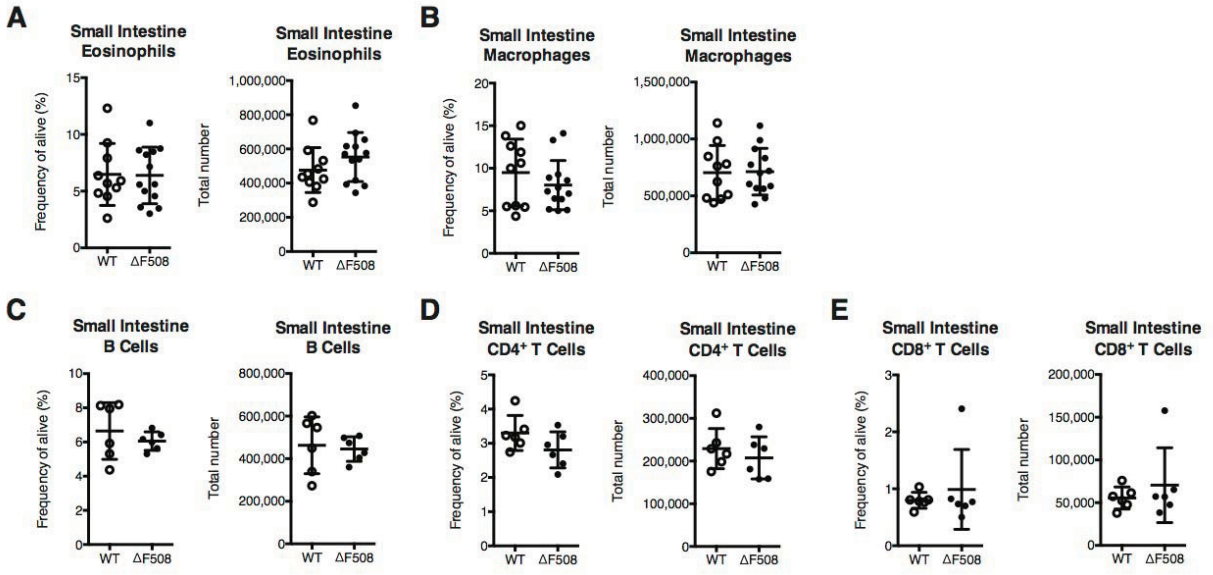

Appendix 3. Immunophenotyping of the small intestine lamina propria at 4DPI with *C. rodentium*. Frequency and total number of: **(A)** SSC^{hi} Siglec-F^{+} eosinophils in the small intestine of ΔF508 (*n* = 13) and WT (*n* = 10) mice at 4DPI with *C. rodentium*. **(B)** $CD11b^{+}$ $F4/80^{+}$ macrophages in the small intestine of ΔF508 (*n* = 13) and WT (*n* = 10) mice at 4DPI with *C. rodentium*. **(C)** $TCR\beta^{-}$ $CD19^{+}$ B cells in the small intestine of ΔF508 (*n* = 6) and WT (*n* = 6) mice at 4DPI with *C. rodentium*. **(D)** $TCR\beta^{+}$ $CD4^{+}$ T cells in the small intestine of ΔF508 (*n* = 6) and WT (*n* = 6) mice at 4DPI with *C. rodentium*. **(E)** $TCR\beta^{+}$ $CD8^{+}$ T cells in the small intestine of ΔF508 (*n* = 6) and WT (*n* = 6) mice at 4DPI with *C. rodentium*.

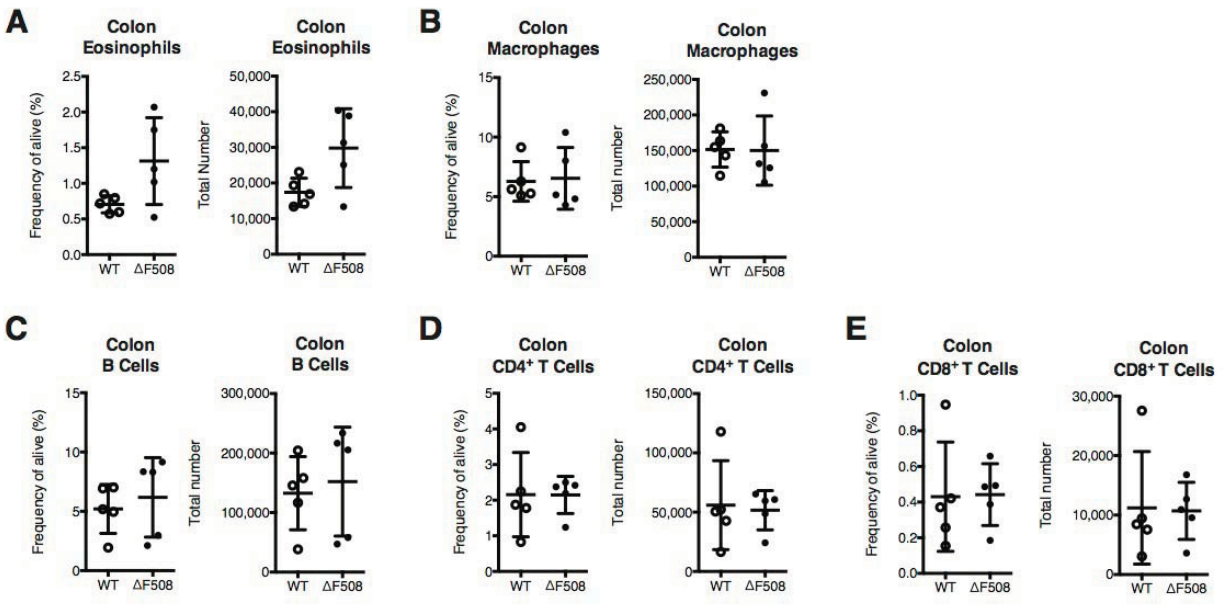

Appendix 4. Immunophenotyping of the colon lamina propria at steady state.
Frequency and total number of **(A)** SSC^{hi} Siglec-F^{+} eosinophils in the colon of ΔF508 (*n* = 5) and WT (*n* = 5) mice at steady state. **(B)** $CD11b^{+}$ $F4/80^{+}$ macrophages in the colon of ΔF508 (*n* = 5) and WT (*n* = 5) mice at steady state. **(C)** $TCR\beta^{-}$ $CD19^{+}$ B cells in the colon of ΔF508 (*n* = 5) and WT (*n* = 5) mice at steady state. **(D)** $TCR\beta^{+}$ $CD4^{+}$ T cells in the colon of ΔF508 (*n* = 5) and WT (*n* = 5) mice at steady state. **(E)** $TCR\beta^{+}$ $CD8^{+}$ T cells in the colon of ΔF508 (*n* = 5) and WT (*n* = 5) mice at steady state.

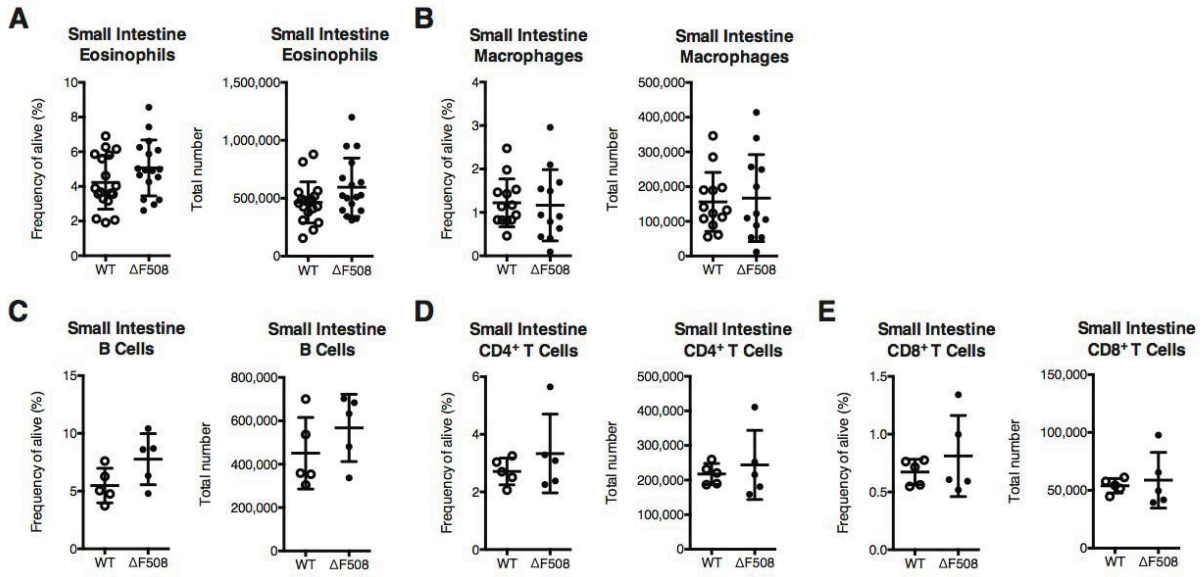

Appendix 5. Immunophenotyping of the small intestine lamina propria at steady state.
Frequency and total number of: **(A)** SSC^{hi} Siglec-F^{+} eosinophils in the small intestine of ΔF508 (*n* = 17) and WT (*n* = 18) mice at steady state. **(B)** $CD11b^{+}$ $F4/80^{+}$ macrophages in the small intestine of ΔF508 (*n* = 17) and WT (*n* = 18) mice at steady state. **(C)** $TCR\beta^{-}$ $CD19^{+}$ B cells in the small intestine of ΔF508 (*n* = 5) and WT (*n* = 5) mice at steady state. **(D)** $TCR\beta^{+}$ $CD4^{+}$ T cells in the small intestine of ΔF508 (*n* = 5) and WT (*n* = 5) mice at steady state. **(E)** $TCR\beta^{+}$ $CD8^{+}$ T cells in the small intestine of ΔF508 (*n* = 5) and WT (*n* = 5) mice at steady state.

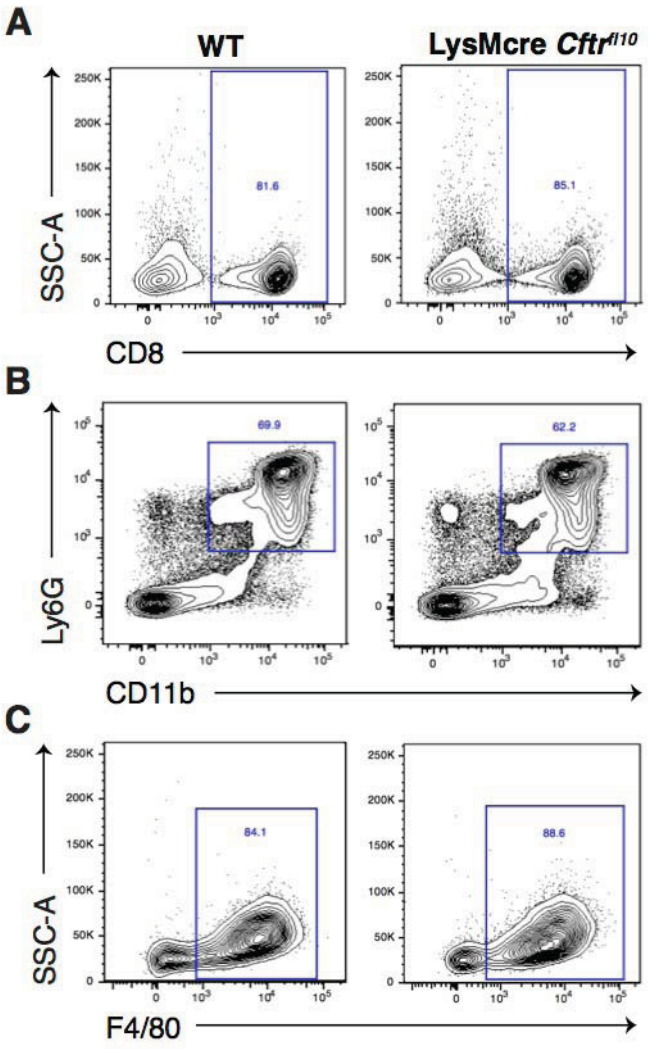

Appendix 6. Assessment of the purity of cell types isolated for confirmation of CFTR excision. Representative contour plot of: **(A)** $CD8^+$ T cells isolated from the spleen of LysMcre *Cftr*^{fl10} and WT mice. Gated on single cells, live cells, $CD45^+$. **(B)** $CD11b^+$ $Ly6G^+$ neutrophils isolated from the bone marrow of LysMcre *Cftr*^{fl10} and WT mice. Gated on single cells, live cells, $CD45^+$. **(C)** $F4/80^+$ macrophages enriched from the bone marrow of LysMcre *Cftr*^{fl10} and WT mice. Gated on single cells, live cells.